https://doi.org/10.5194/egusphere-2026-3147
Preprint. Discussion started: 25 June 2026

Evolution of aerosol composition and optical properties in the Paris urban plume from coordinated airborne and ground-based observations

Chenjie Yu[1], Ludovico Di Antonio[2,a], Peter F. DeCarlo[3], Benjamin A. Nault[3,4], Alejandra Velazquez-Garcia[5], Eleonora Aruffo[6,7], Piero Di Carlo[7,8], Cyrielle Denjean[5], Sarah Tinorua[5,b], Thierry Bourrianne[5], Diana L. Pereira[1,c], Kevin Tu[2,d], Edouard Pangui[2], Mathieu Cazaunau[2], Astrid Bauville[2,e], Noël Grand[1], Antonin Bergé[2,f], Claudia Di Biagio[1], Aline Gratien[1], Matthias Beekmann[1], Guillaume Siour[2], Gilles Foret[2], Barbara D'Anna[9], Julien Kammer[9], Huihui Wu[1,10], Christopher Cantrell[2], Paola Formenti[1], and Vincent Michoud[1]

[1]Université Paris Cité and Univ Paris Est Créteil, CNRS, LISA, F-75013 Paris, France
[2]Univ Paris Est Créteil and Université Paris Cité, CNRS, LISA, 94010 Créteil, France
[3]Department of Environmental Health and Engineering, Whiting School of Engineering, Johns Hopkins University, Baltimore, Maryland, USA
[4]Center for Aerosol Cloud and Chemistry, Aerodyne Research, Inc., Billerica, Massachusetts, USA
[5]Météo France, CNRS, Univ. Toulouse, CNRM, Toulouse, France
[6]Department of Science, University "G.d'Annunzio" of ChietiPescara, Chieti 66100, Italy
[7]Center for Advanced Studies and Technology (CAST), Chieti 66100, Italy
[8]Department of Advanced Technologies in Medicine & Dentistry, University "G.d'Annunzio" of ChietiPescara, Chieti 66100, Italy
[9]Aix Marseille Univ, CNRS, LCE, Marseille, France
[10]Department of Earth and Environmental Sciences, University of Manchester, Manchester M13 9PL, United Kingdom
[a]Now at: LATMOS/IPSL, Sorbonne Université, UVSQ, CNRS, 75252 Paris, France
[b]Now at: PSI Center for Energy and Environmental Sciences, 5232 Villigen PSI, Switzerland
[c]Now at: Institute for Atmospheric and Earth System Research/Physics, Faculty of Science, University of Helsinki, Helsinki, Finland
[d]Now at: Safran Aircraft Engines/Akkodis, 77550 Moissy-Cramayel, France
[e]Now at: Muséum national d'Histoire naturelle (MNHN, CNRS), BioArch, Paris, France
[f]Now at: Laboratoire des Sciences du Climat et de l'Environnement, CEA–CNRS–UVSQ, IPSL, Université Paris-Saclay, 91191 Gif-sur-Yvette, France

Correspondence to: Chenjie Yu (chenjie.yu@lisa.ipsl.fr) and Paola Formenti (paola.formenti@lisa.ipsl.fr)

Abstract.

Aerosols play a critical role in Earth's climate, but substantial evolution in their physicochemical properties after emission introduces uncertainties in predicting their climate impacts. Observational constraints on how aging modifies aerosol properties remain limited. Here, we investigate the effects of ~2–6 h of aging on aerosol physicochemical properties using coordinated airborne and ground-based measurements in Paris and its downwind regions. Urban plumes contributed modestly to particle number concentrations in the 80–200 nm size range and resulted in a moderate enhancement of submicron particle (PM_1) mass relative to out-plume background levels. Organic aerosol (Org) dominated PM_1 mass both near the urban source and downwind. Aircraft observations showed enhanced Org and non-refractory PM_1 relative to excess CO (CO above surrounding background)

https://doi.org/10.5194/egusphere-2026-3147
Preprint. Discussion started: 25 June 2026

in downwind plumes, indicating net secondary organic aerosol production during aging. Aerosol optical properties evolved concurrently. Downwind plume-average single-scattering albedo (SSA) at 450 and 630 nm was higher than near-source values. Consistently, the complex refractive index shifted from lower real (~1.35–1.40) and higher imaginary (~0.03–0.08) components near source to higher real (~1.45–1.50) and lower imaginary (~0.015–0.02) components downwind. The absorption Ångström exponent also increased, indicating a greater fractional contribution of brown carbon to light absorption. These results demonstrate that urban plume aging alters aerosol composition and optical properties and highlight the need to represent evolving aerosol characteristics in atmospheric models and remote-sensing retrievals.

1. Introduction

Atmospheric aerosols play an important role in regulating climate through their interactions with radiation and clouds (Farmer et al., 2015; Ravishankara et al., 2015). Atmospheric aerosols also degrade air quality by impairing visibility, posing risks to human health, particularly the respiratory system, and exerting adverse impacts on natural ecosystems (Manisalidis et al., 2020). Urban areas are major sources of anthropogenic emissions and contribute substantially to aerosol burdens through activities such as transportation, industrial processes, and residential energy use (Karagulian et al., 2015). Previous studies have shown that organic aerosol (OA) constitutes a substantial fraction of total submicron particulate matter in urban environments worldwide (Zhang et al., 2007; Jimenez et al., 2009; Nault et al., 2021), with nitrate also making an important contribution compared to remote regions (Li et al., 2018). The chemical composition of urban aerosols and their associated physicochemical properties evolve continuously after emission during atmospheric aging. These aging processes, including coagulation, secondary species formation, and heterogeneous reactions, can substantially alter aerosol composition, size distribution, mixing state, optical properties, and cloud condensation nuclei (CCN) activity, thereby influencing their impacts on air quality and climate (Zaveri et al., 2010; Riemer et al., 2019).

Observational studies are essential for characterizing the evolution of urban aerosol physicochemical properties. Ground-based observations provide important insights into the temporal variability of aerosol physicochemical properties at fixed locations. Previous measurements at urban sites show that secondary organic aerosol (SOA) constitutes a substantial fraction of the organic aerosol (OA) budget in the urban environments (Chen et al., 2022), and that its rapid formation is predominantly driven by photochemical processes (Hayes et al., 2013). However, ground-based observations often represent a mixture of fresh and aged aerosols and therefore have limited ability to isolate the aerosol aging process within urban plumes. Airborne measurements offer a unique capability to directly sample urban plumes at different distances from their emission sources, enabling the investigation of aerosol evolution as a function of transport time and atmospheric processing (Kahn et al., 2023). Airborne observations over the megacities around the world (Freney et al., 2014; Nault et al., 2018; DeCarlo et al., 2010; Schroder et al., 2018) have revealed a rapid transformation of urban aerosol compositions during the plume aging in both

https://doi.org/10.5194/egusphere-2026-3147
Preprint. Discussion started: 25 June 2026

summer and winter. Specifically, within a few hours downwind of urban plumes, the fraction of primary organic aerosol (hydrocarbon-like organic aerosol) decreases in total PM_1 organic matter, while the fraction of secondary organic aerosol (oxygenated organic aerosol) increases correspondingly. Furthermore, Shilling et al. (2018) reported that even in environments with strong regional background SOA contributions, rapid SOA formation is still observed within a few hours of transport downwind of urban plumes.

Such efficient compositional changes within urban plumes are closely linked to the evolution of aerosol climate-relevant properties. Zaveri et al. (2022) demonstrates that the rapid SOA formation during urban plume aging in the Amazon region plays an important role in particle growth and CCN formation. McMeeking et al. (2012) reported an increase in the single-scattering albedo (SSA) at 550 nm downwind of the London urban plume, which is attributed to the increasing formation of secondary, non-light-absorbing aerosol components during plume aging. Dingle et al. (2016) observed enhanced aerosol extinction coefficients at 632 nm within aged urban plumes compared with fresh plumes, associated with the SOA formation during the plume aging. These changes in aerosol optical properties are fundamentally governed by the complex refractive index (CRI), which links aerosol chemical composition and mixing state to its optical behaviour and ultimately to radiative effects. As secondary aerosol formation modifies the relative contributions of scattering and absorbing components, it alters both the real and imaginary parts of the CRI, thereby influencing aerosol extinction and absorption (Wu et al., 2021; He et al., 2021). Despite its central role, observational constraints on the evolution of aerosol chemical composition and effective CRI after emission from urban regions remain limited. Chemical transport models often misrepresent aerosol chemical compositions near and downwind of anthropogenic source regions (Tsigaridis et al., 2014; Zhang et al., 2015; Jathar et al., 2017). Consequently, substantial uncertainties remain in simulating the evolution of aerosol optical properties, as models typically rely on prescribed CRI values for individual aerosol components and simplified mixing-state assumptions, which may not adequately capture their dynamic evolution during aerosol aging (Tsigaridis and Kanakidou, 2018; Brown et al., 2021). In addition, many aerosol remote sensing retrieval methods employ simplified aerosol models with prescribed optical properties (e.g. Grzegorski et al. (2022); Zhang et al. (2025)) or predefined optical properties for each aerosol component (e.g. Li et al. (2022b)). As a result, deviations between these assumptions and the actual evolution of aerosol optical properties may introduce uncertainties in retrieved aerosol optical depth (AOD), SSA, and aerosol type classification. In this context, in-situ observations of aerosol CRI provide valuable constraints for evaluating these assumptions and improving the representation of aerosol optical properties in both satellite retrieval algorithms and atmospheric models.

The Greater Paris region (Île-de-France) is a densely populated European megacity with substantial anthropogenic emissions, where aerosols play an important role in regional climate impacts and air quality according to the previous experiments (Beekmann et al., 2015). Characterizing the evolution of aerosol physicochemical properties within urban plumes is therefore essential for understanding the relative contributions of primary emissions and secondary formation, as well as their impacts on climate-relevant properties. Previous airborne measurement (Freney et al., 2014) shows that the Paris urban plume is mainly

https://doi.org/10.5194/egusphere-2026-3147
Preprint. Discussion started: 25 June 2026

composed of OA, BC, and particulate nitrate (pNO_3), and SOA formation is largely driven by anthropogenic gas-phase precursors. However, the impacts of the evolution of aerosol chemical components on aerosol optical properties within Paris urban plume are not addressed. Moreover, these airborne measurements were conducted more than a decade ago. In recent years, ozone (O_3) has become a prominent pollutant in many European urban environments. Declining nitrogen oxide (NO_x) emissions have been linked to rising urban O_3 levels (Grange et al., 2021), suggesting changes in atmospheric oxidative capacity and underscoring the need to re-examine the evolution of aerosol physicochemical properties during transport under current chemical conditions.

In this study, we focus on characterising the evolution of aerosol chemical and optical properties within the Paris urban plume by combining airborne and ground-based observations. Aircraft measurements conducted within the boundary layer are used to intercept the urban plume after emission, providing direct observations of aerosol physicochemical properties at transport ages of only a few hours. Simultaneous ground-based measurements in the Paris central urban area are employed to characterize near-source aerosol properties for qualitative comparison. The results provide insight into the evolution of aerosol optical properties in the surrounding of a major European megacity and their association with aerosol chemical composition, with implications for air quality and climate.

2. Experiment Methods and data analysis

2.1 Atmospheric Chemistry of the Suburban Forest (ACROSS) project

This study focuses on measurements obtained from aircraft observations and a ground-based site within the Atmospheric Chemistry of the Suburban Forest (ACROSS) project which provided with a broad range of observations of gas- and aerosol-phase species over the Greater Paris region (Cantrell and Michoud, 2022). A summary of the instruments used in this study and their availability together with their measurement frequencies is provided in Table S1 in the Supplementary. To enable comparison between aircraft observations and ground-based measurements, all results were reported under standard temperature and pressure (STP) conditions (T = 273.15 K, P = 1013.25 hPa) in this study.

The French environmental research aircraft SAFIRE (Service des Avions Français Instruments pour la Recherche en Environnement) ATR-42 was used to sample the evolution of Paris urban plume as part of the ACROSS project. The aircraft conducted zigzag transects across the Paris urban plume within the boundary layer at ~300–400 m above ground level (a.g.l.). The airborne measurement was performed between 13th June and 7th July, 2022 and the flight paths are presented in Figure 1. In this study, a total of 8 flights is selected based on the availability and operational status of the instruments.

https://doi.org/10.5194/egusphere-2026-3147
Preprint. Discussion started: 25 June 2026

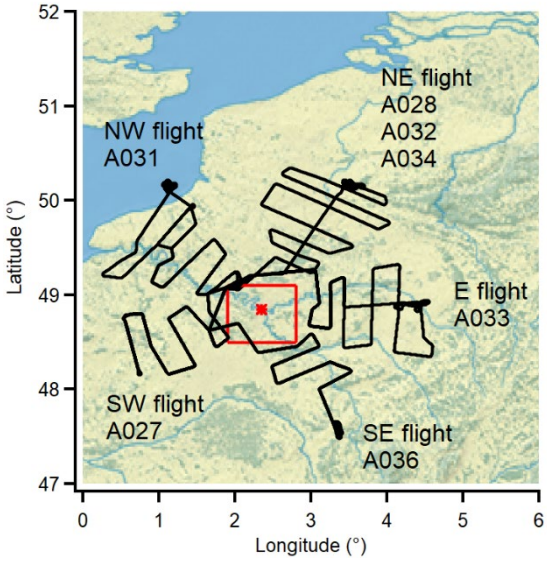

Figure 1. Flight paths of the selected ACROSS flights during the campaign. The red marker indicates the PRG site in central Paris, and the red square outlines the Greater Paris region (Île-de-France). The ATR-42 departed from Cergy Airport, located in the northwestern Greater Paris region, and conducted zigzag flight transects across the Paris urban plume. Maps were created from public domain GIS data on Natural Earth (http://www.naturalearthdata.com, last access: 01/04/2026).

The ground-based site used in this study is the Paris Rive Gauche (PRG) site (48.83° N, 2.38° E) which located at Université Paris Cité in the central part of the Greater Paris Region (Di Antonio et al., 2025). The PRG measurement site was located a few hundred meters away from major traffic emission sources, including train stations and urban highways. The measurements were conducted on the roof of the university building which was 30 m a.g.l. In this study, observations from the PRG measurement site were used as reference conditions for the initial particulate and gas-phase pollutant emissions of the Paris urban plume. The emission periods selected from the PRG measurements were determined using back-trajectory analysis, as described in Section 2.5.

2.2 SAFIRE aircraft instrumentations

2.2.1 Airborne particulate-phase measurements

A mini-Aerosol Mass Spectrometer (mAMS, Aerodyne Research, Inc.) was used to characterise the non-refractory submicron Particulate Matter (NR-PM_1) compositions and mass concentrations, including OA, sulfate (SO_4), pNO_3, ammonium (NH_4), and chloride (Chl). Note, charges are not included for the inorganic aerosol as the evaporation and fragmentation of the aerosol leads to observing both organic and inorganic species within the SO_4, pNO_3, NH_4, and Chl family (Chen et al., 2019; Farmer et al., 2010). The mAMS has been successfully deployed in mobile ground-based (Goetz et al., 2018; Goetz et al., 2022; Werden et al., 2023) and airborne measurements (Vu et al., 2016; Konwar et al., 2024). Briefly, the mAMS is a miniaturized

https://doi.org/10.5194/egusphere-2026-3147
Preprint. Discussion started: 25 June 2026

version of the standard compact Time-of-Flight AMS (c-ToF-AMS, Aerodyne Research, Inc.) (Drewnick et al., 2005), while maintaining comparable analytical performance. Key modifications of the mAMS compared to the standard c-ToF-AMS include a smaller vacuum chamber, and the integration of a single split-flow turbo molecular pump from the ToF Aerosol Chemical Speciation Monitor (ToF-ACSM, Aerodyne Research, Inc.) (Fröhlich et al., 2013). The mAMS measures NR-PM_1 compositions by focusing particles into a narrow beam with a critical orifice and aerodynamic lens. When particles impact on a heated metallic surface (~ 600℃), the NR-PM_1 components are vaporized, subsequently ionized by 70 eV electron impact, and quantitatively detected by ToF-MS under high vacuum. The Ionization Efficiency (IE) of the mAMS was calibrated using mono-disperse, nebulized ammonium nitrate particles at 300 nm. Default Relative Ionization Efficiency (RIE) was applied for each compound, and a constant Collection Efficiency (CE) 0.5 was applied to the final ambient results. To meet the short intercept time of Paris urban plume, the mAMS was operated in Fast mass spectrum (FMS) mode with 1 s frequency. The final results were averaged to 15s to improve the signal-to-noise ratio. The total volume of NR-PM_1 estimated from mAMS, assuming densities of 1.27 g cm^{-3} for Org and 1.77 g cm^{-3} for inorganics (Cross et al., 2007), was comparable to that derived from the particle size distribution instrument. The comparison is presented in Figure S1 in the Supplementary Information, showing a slope of 0.75 between the two measurements and a correlation coefficient (R^2) of 0.82.

The refractory black carbon (rBC)-containing particles were characterized by a Single Particle Soot Photometer (SP2, DMT). The term rBC defined here is following the definition in Petzold et al. (2013). Briefly, the SP2 employs a 1064 nm Nd:YAG crystal laser and a set of optical detectors, including scattering detectors and incandescence detectors. When an rBC-containing particle passes through the laser beam, it absorbs laser energy and becomes heated to incandescence, emitting thermal radiation in the visible to near-infrared range. The incandescence detectors then capture this signal and unambiguously identify the particle as rBC. The SP2 detects rBC components with an equivalent spherical diameter in the range of 90-580 nm. The SP2 was calibrated with mono-disperse, nebulized standard soot particles (Alfa Aesar, lot no. FS12S011) to establish the calibration ratio between particle mass concentrations and the strength of the instrument signal, and a density of 1.8 g cm^{-3} was applied to rBC (Taylor et al., 2015). SP2 data were processed using the SP2Py-Pro toolkit (Tinorua et al., 2024a; Velazquez-Garcia et al., 2026)

The aerosol extinction and scattering coefficients at 450 nm ($\sigma_{\mathrm{ext,450\ nm}}$ and $\sigma_{scat,450\ \mathrm{nm}}$, respectively, units of $Mm^{-1} = 10^{-6}$ m^{-1}) and 630 nm ($\sigma_{\mathrm{ext,630\ nm}}$ and $\sigma_{scat,630\ \mathrm{nm}}$, respectively) were measured through the A2S2 (Aerosol Absorption Spectral Sizer, custom built), a custom-built airborne dual-wavelength cavity-attenuated phase shift single-scattering albedo monitor (CAPS-PM_{SSA}, Aerodyne Research, Inc.) developed at LISA (CNRS), as described in detail by Yu et al. (2024). The design of the CAPS-PM_{SSA} is described in Onasch et al. (2015). Briefly, the instrument uses a high-reflectivity optical cavity (~99.99%) with an LED light source (450 and 630 nm for A2S2 used in this study), where σ_{ext} is derived from the phase shift change of a square-wave modulated beam when particles are present relative to a particle-free baseline. σ_{scat} is measured with an integrated sphere coated with highly reflective material acting as a nephelometer, with scattered light detected by a

https://doi.org/10.5194/egusphere-2026-3147
Preprint. Discussion started: 25 June 2026

photomultiplier tube (PMT) to maximize light collection and minimize truncation biases. The absorption coefficient (σ_{abs}) is derived from the Extinction-Minus-Scattering (EMS) method (Weber et al., 2022). Prior to the flight campaign, the A2S2 scattering channels were calibrated using aerosolised 200 nm polystyrene latex (PSL) particles (Single Scattering Albedo (SSA) = 1), in accordance with the CAPS-PM$_{SSA}$ calibration protocol. Both $\sigma_{scat,450\,nm}$ and $\sigma_{scat,630\,nm}$ were corrected for angular truncation using a wavelength-dependent correction based on the Scattering Ångström exponent (SAE), following the method described by Yu et al. (2024).

An Ultra-High Sensitivity Aerosol Spectrometer (UHSAS) was used to derive the particle size distribution between 40 – 1000 nm. However, considering the elevated uncertainty in the smallest UHSAS size channels near the detection limit, the first bins were excluded and only the 80 – 1000 nm size range was analysed. The coarse mode particle size distributions (~0.08 – ~10 µm) were obtained through an Optical Particle Counter (Sky-OPC, GRIMM Inc, model 1.129). The combined size distribution was constructed by merging the UHSAS and Sky-OPC datasets, with the transition between instruments defined at 1 µm. UHSAS and Sky-OPC optical diameters were converted to equivalent geometric diameters assuming the CRI of polystyrene latex (PSL; CRI = 1.59) at the instrument operating wavelengths (1054 nm for the UHSAS and 655 nm for the Sky-OPC), respectively. Cloud droplet size distributions between 2 and 50 µm were measured using a Cloud Droplet Probe (CDP, DMT). The CDP results were used to identify in-cloud periods, defined as periods when the liquid water content (LWC) exceeded 0.01 g m^{-3}. The LWC was calculated from the droplet size distributions assuming a liquid water density of 1 g cm^{-3}. All data corresponding to in-cloud conditions were excluded from the analysis.

Onboard the aircraft, the Sky-OPC, A2S2 and SP2 were connected to the AVIRAD measurement system, consisting an isoaxial and isokinetic inlet located below the aircraft and characterised by a collection efficiency of 50% at 12 µm in particle optical diameter (Formenti et al., 2011). The mAMS was connected to a Rosemount inlet mounted on the side of the fuselage via a stainless-steel sampling line, providing near-unity transmission efficiency for submicron particles (Capes et al., 2008). The stainless-steel sampling line between the mAMS and the Rosemount inlet was ~1 m, corresponding to an estimated residence time of ~0.6 s, and the influence of residence time on the measured aerosol composition is expected to be negligible. Although no dryer was used upstream of these instruments onboard the aircraft, the RH measured at the inlet remained below 40% during the selected airborne measurement periods due to ram heating (presented in Table S6 in the Supplementary Information). Thus, the measurements were considered to represent near-dry aerosol conditions.

2.2.2 Airborne gas-phase measurements

NO_2 measurements were conducted using a four-channel Thermal Dissociation Laser Induced Fluorescence (TD-LIF). Details of the TD-LIF principles and its airborne deployment are provided in Di Carlo et al. (2013). The instrument detects NO_2 via laser-induced fluorescence following excitation at 532 nm, while additional total gas-phase nitrogen species (NO_y) species are quantified through controlled thermal dissociation in parallel heated channels. Total Peroxy Nitrates (ΣPNs), total Alkyl

https://doi.org/10.5194/egusphere-2026-3147
Preprint. Discussion started: 25 June 2026

Nitrates (ΣANs), and nitric acid (HNO_3) are thermally decomposed into NO_2 at approximately 200°C, 350°C, and 600°C, respectively, with the resulting NO_2 subsequently measured by LIF. The TD-LIF was calibrated using standard cylinder of NO_2 and zero air. However, TD-LIF measurements were not available during Flight A036, and NO_2 was instead measured using a CAPS-NO_2 instrument (Teledyne, T500U). The CAPS-NO_2 was calibrated before and after the campaign using the same procedure as for the TD-LIF instrument. Owing to the faster response time and lower detection limit of TD-LIF compared to CAPS-NO_2 (as described in Table S1 in the Supplementary Information), absolute NO_2 concentrations reported in this study were based on TD-LIF measurements. The CAPS-NO_2 data for Flight A036 were used only in a relative sense to identify plume periods, and the corresponding absolute NO_2 concentrations were not included in the final analysis. O_3 was measured through an ozone analyser (Thermo Scientific, Model 49i), and CO was measured through an in-flight gas concentration analyser (PICARRO, G2401-m). The background CO was defined as the 5th percentile of each flight.

2.2.3 Airborne meteorological parameter measurements

The air temperature and relative humidity (RH) were measured through a Rosemount housing (E102AL Rosemount) and a 1011C hygrometer onboard the aircraft, respectively. Horizontal wind speed and direction were derived from a combination of airspeed and flow angle measurements from a nose-mounted gust probe and aircraft motion data from the onboard inertial navigation system (INS)/GPS. The results of average meteorological parameters for each flight are presented in Table S6 in the Supplementary Information.

2.3 Ground based measurements in Paris urban site

At PRG ground-based site, a ToF-ACSM was used to characterise the NR-PM_1 compositions. The ACSM measures the chemical composition of NR-PM_1 using principles similar to those of the mAMS, including aerodynamic focusing, thermal vaporization, and electron-impact ionization. Ammonium nitrate and ammonium sulfate was used to do the calibrations. The IE of ACSM has also been calibrated using mono-disperse, nebulized ammonium nitrate particles at 300 nm. The RIE of NH_4 and SO_4 for the ACSM were determined from measurements of 300 nm ammonium nitrate and ammonium sulfate particles, respectively. A constant CE 0.5 was applied to the final ambient results. It should be noted that signals at specific mass-to-charge (m/z) ratios derived from mAMS and ACSM measurements are not strictly comparable, as differences in instrument design and operating principles (e.g., vaporization and sampling protocols) can introduce systematic variations in the measured signals (Pieber et al., 2016). Therefore, detailed comparisons of individual m/z signals (e.g., m/z 44 and 43) between mAMS and ACSM were not considered in this study.

The σ_{scat} of PM_1 particles at 450, 550 and 700 nm was measured through a Nephelometer (NEPH, Ecotech Aurora 4000), while the σ_{abs} of PM_1 at seven different wavelengths (370, 470, 520, 590, 660, and 880 and 950 nm) was measured by a dual-spot aethalometer (AE33, Magee Sci.) (Yus-Díez et al., 2021). Details of the PRG optical instrumentation and data analysis are described in Di Antonio et al. (2025). NEPH measures the aerosol scattering coefficient by illuminating an aerosol sample

https://doi.org/10.5194/egusphere-2026-3147
Preprint. Discussion started: 25 June 2026

with a collimated light source and detecting the light scattered by particles over a range of angles ($9-170^{\circ}$) using photodetectors. Correction of the NEPH truncation error was performed according to the submicron aerosol formulation described by Teri et al. (2022). The AE33 measures the light attenuation coefficient (σ_{atn}) through a filter tape, which was sampled at 1-minute intervals. The spectral aerosol absorption coefficient is determined as:

$$\boldsymbol{\sigma_{\mathrm{abs}} = \frac{\sigma_{\mathrm{atn}}}{C_{\mathrm{ref}}}} \qquad (1)$$

Where C_{ref} is the multiple scattering correction factor. While the filter-based AE33 quantifies σ_{abs} via transmittance attenuation from deposited particles, its accuracy is compromised by multi-scattering interactions within the filter matrix, including variable aerosol loading and filter leakage. A wavelength-independent C_{ref} of 2.45 has been applied to correct the final absorption coefficient results as recommended by ACTRIS (Savadkoohi et al., 2023). The light absorbing equivalent Black Carbon (eBC) mass concentration is derived from the multiple scattering corrected 880 nm channel results using a mass absorption cross section (MAC) of 7.77 $m^2\ g^{-1}$ (Petzold et al., 2013; Bond et al., 2013). As BC was characterized using different definitions, reported as eBC by the AE33 at PRG and as rBC by the SP2 onboard the aircraft, their absolute mass concentrations are not directly comparable. A simplified factor of 2 was applied to convert eBC mass concentrations to rBC, following Tinorua et al. (2024b) and Laing et al. (2020), and the converted AE33 rBC mass concentration results were only used to illustrate the relative changes in the rBC mass fraction (presented in Figure S2 in the Supplementary Information). The σ_{scat} measured by NEPH and the σ_{abs} measured by AE33 have been scaled to match the airborne A2S2 wavelengths, as described in Section 2.4. The σ_{ext} of PM_1 at 450 and 630 nm was then calculated as the sum of σ_{scat} and σ_{abs} at the corresponding wavelengths. Yu et al. (2024) has demonstrated that the σ_{scat}, σ_{abs} and σ_{ext} at 450 and 630 nm derived from A2S2 agree well with measurements from the NEPH and AE33, respectively, across a range of aerosol loading conditions. Weber et al. (2022) similarly demonstrated that CAPS-PM_{SSA} measurements are comparable to those from NEPH and other optical instruments at these wavelengths. These findings support the intercomparison of airborne and PRG optical properties in this study.

The particles size distribution at PRG was measured through a Scanning Mobility Particle Sizer (SMPS) which consists of a Differential Mobility Analyzer (DMA, TSI model 3082) and a Condensation Particle Counter (CPC, TSI model 3776). Sheath and aerosol flow were fixed at 3.0 L min^{-1} and 0.3 L min^{-1}, to measure particle size distribution across 23-982 nm range, with one scan measured every 2 minutes. The SMPS mobility diameters were interpreted as equivalent geometric diameters by assuming spherical particles with a shape factor of 1.

All aerosol measurement instruments (ACSM, SMPS, AE33, and NEPH) were connected to a PM_1 sampling head. A Nafion dryer was applied before the ACSM. Air was drawn through a 10 m copper tube from the PM_1 inlet to a four-way stainless-steel flow splitter (TSI) located in the measurement room, which distributed the airflow to the individual instruments. Losses by diffusion were calculated individually for each instrument using Particle Loss Calculator (PLC, developed by Max Plank

https://doi.org/10.5194/egusphere-2026-3147
Preprint. Discussion started: 25 June 2026

Institute; (Von Der Weiden et al., 2009) as a function of the geometry (curvature and pipes size) of sampling lines and aerosol properties (Baron and Willeke, 2001).

NO_2 was measured by an ozone chemiluminescence analyzer (model AC32M, Envea), and O_3 was measured through a UV-absorption monitor (model O3-41M, Envea). More details of the gas-phase measurements at PRG are described in Pereira et al. (2025). The CO data were taken from the closest AIRPARIF (Association Interdépartementale pour la gestion du Réseau automatique de surveillance de la Pollution Atmosphérique et d'Alerte en Région d'Île-de-France) monitoring site, situated in central Paris (Châtelet–Les Halles), at a distance of ~6 km from the PRG site location. The background CO concentration for each day was assumed to be identical to that derived from the corresponding flight, since the aircraft measurements were conducted within the boundary layer and were therefore representative of near-surface conditions.

2.4 Optical properties evaluation and derivation of the dry aerosol complex refractive index (CRI)

For comparisons at the consistent wavelengths with the airborne A2S2 wavelengths, the PRG NEPH and AE33 results have been scaled using the Ångström exponent approach using equation (3):

$$\boldsymbol{xAE} = -\frac{\ln(\sigma_{\lambda_1}/\sigma_{\lambda_2})}{\ln(\lambda_1/\lambda_2)} \quad (2)$$

Where xAE is the Scattering or Absorption Ångström Exponent (SAE, AAE), σ_{λ_1} and σ_{λ_2} represent the scattering or absorption coefficient at wavelengths λ_1 and λ_2 respectively. The absorption or the scattering coefficient (σ_λ) at a given wavelength (λ, 450 or 630 nm) can be derived through equation (4):

$$\boldsymbol{\sigma_\lambda} = \boldsymbol{\sigma_{\lambda_0}} \cdot \left(\frac{\lambda}{\lambda_0}\right)^{-\mathbf{xAE}} \quad (3)$$

Where σ_{λ_0} is the absorption or scattering coefficient at the wavelength λ_0. In this study, the σ_{sca} at 630 nm for the NEPH is derived through measurements at 700 nm, and the σ_{abs} at 450 and 630 nm for the AE33 is derived through absorption measurements at 470 and 660 nm, respectively.

The BrC absorption coefficient is determined in the assumption that absorption at 630 nm is contributed by BC only and the AAE for BC is 1. Henceforth, the σ_{abs} contributed by BC at 450 nm can be derived as:

$$\boldsymbol{\sigma_{\text{abs BC},450}} = \boldsymbol{\sigma_{\text{abs},630}} \cdot \left(\frac{450}{630}\right)^{-\boldsymbol{AAE_{450/630}}} \quad (4)$$

Then the σ_{abs} of BrC at 450 nm can be estimated as:

$$\boldsymbol{\sigma_{\text{abs BrC},450}} = \boldsymbol{\sigma_{\text{abs},450}} - \boldsymbol{\sigma_{\text{abs BC},450}} \quad (5)$$

The Single Scattering Albedo (SSA) at 450 and 630 nm is derived from the ratio between σ_{scat} and σ_{ext} at each wavelength:

$$\boldsymbol{SSA_\lambda} = \frac{\boldsymbol{\sigma_{scat,\lambda}}}{\boldsymbol{\sigma_{ext,\lambda}}} \quad (6)$$

https://doi.org/10.5194/egusphere-2026-3147
Preprint. Discussion started: 25 June 2026

The complex refractive index (CRI) is estimated using a size-integrated optical closure approach based on aerosol size distribution and optical properties measurements (same as the CRI estimation method described in Di Antonio et al. (2025)). Mie theory is applied to calculate the aerosol scattering and absorption coefficients for a range of prescribed CRI, with the real part (n) varying from 1.2 to 1.8 (at 0.01 step) and the imaginary part (k) from 0 to 0.02 (at 0.001 step). For each prescribed CRI pair ($n + ki$), the simulated scattering and absorption coefficients are compared with the corresponding observations, and the root mean square difference (RMSD) is computed as the cost function:

$$\boldsymbol{RMSD} = \sqrt{\left(\frac{\sigma_{scat,model}-\sigma_{scat,measure}}{\sigma_{sca,model}}\right)^2 + \left(\frac{\sigma_{abs,model}-\sigma_{abs,measure}}{\sigma_{abs,model}}\right)^2} \qquad (7)$$

Where $\boldsymbol{\sigma_{scat,model}}$ and $\boldsymbol{\sigma_{scat,measure}}$ represent the modelled and measured scattering coefficient, respectively; $\boldsymbol{\sigma_{abs,model}}$ and $\boldsymbol{\sigma_{abs,measure}}$ represent the modelled and measured absorption coefficient, respectively. The CRI pair that minimizes the RMSD is selected as the optimal solution.

At the PRG site, the optical measurements were constrained to the PM_1 size range. Therefore, the SMPS results were used to determine the size-resolved number concentration (Di Antonio et al., 2025). For the airborne observations, the size distribution was constructed from the combined UHSAS (from ~0.08 to 1 μm) and Sky-OPC (from ~1 to ~10 μm) measurements, ensuring coverage of the full particle size range relevant to A2S2 measurements.

2.5 Paris plume periods identification and transportation age estimation

Intercepts of the Paris urban plume were detected in the airborne measurements based on statistically significant increases (confirmed by a t-test, $p < 0.05$) in both NO_2 and CO mixing ratios observed onboard the ATR-42 aircraft. When SP2 measurements were available, concurrent enhancements in rBC mass concentration within the identified plumes further supported the validity of the is identification approach. The background period was defined as the 5-min interval before and after the plume period, with a 1-min transition interval applied to avoid contamination from the plume. Figure 2(a) presents an example of an identified plume and background period from the Flight A028 on 23rd June, 2022.

The intercepts of the Paris urban plume were further confirmed by a back trajectory analysis. Back trajectories were computed every 15s along the plume period using the UK Met Office Numerical Atmospheric-dispersion Modelling Environment (NAME) model (Jones et al., 2007), driven by meteorological fields from the UK Met Office Unified Model. NAME outputs 24-hour back trajectories on a 0.01° × 0.01° grid by releasing and tracking ensembles of Lagrangian particles, with their historical positions output at 15-min intervals. The 24-hour trajectories are subsequently used to determine whether the sampled air masses have passed over the Greater Paris Region. The wind direction in the meteorological fields was validated against wind direction measurements onboard the aircraft. Figure 2(b) presents the back trajectory results from the same identified plume period from the same flight (Flight A028).

https://doi.org/10.5194/egusphere-2026-3147
Preprint. Discussion started: 25 June 2026

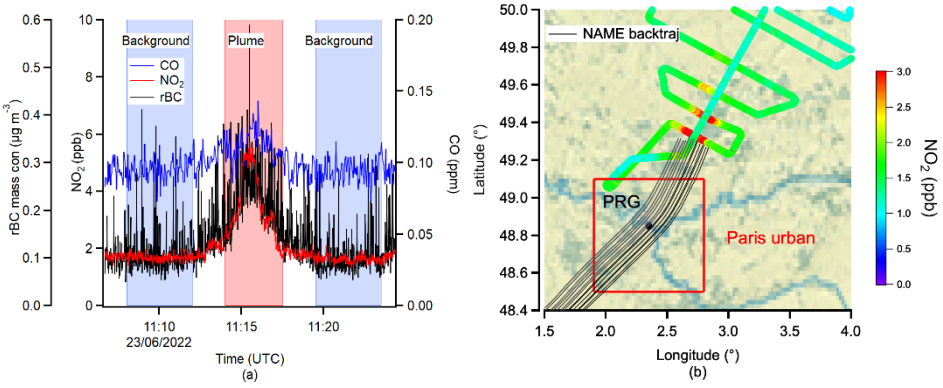

Figure 2. (a) An example of an airborne measured Paris urban plume identified by measured concentrations of NO_2 and CO from the Flight A028 on Jun 23rd, 2022; (b) Back trajectory analysis for the same plume event. Maps were created from public domain GIS data on Natural Earth (http://www.naturalearthdata.com, last access: 01/04/2026).

Once this criterion satisfied, the transport age was derived from the backward trajectories as the time difference between the airborne plume intercept and the point at which the back-tracked particles reached their closest approach to the PRG measurement site. Only the first two plume intercepts encountered during the zigzag flight transects were considered, with an average estimated transport age of less than 6 h. This selection helps reduce the influence of fresh emissions originating from municipalities or industrial sites surrounding the Greater Paris Region. This approach also enables the identification of the urban plume intercepts in flights with lower pollution loading (as Flight A031, A033 and A034 presented in Figure 3), when pollutants concentrations became too low due to dilution. Table S2 in the Supplementary Information summarizes the identified plume periods during the airborne measurements together with the corresponding estimated emission times originating from central Paris. All the PRG results presented in this study are based on data selected within the corresponding emission time windows for the plume periods identified in each flight.

Flights including both outbound and inbound plume interceptions are divided into two case studies, labelled (a) and (b), respectively, as they corresponded to distinct emission periods from the Paris urban centre. The outbound interceptions were mainly associated with the morning traffic rush hour (04:00 – 08:00 UTC) at the PRG site, whereas the inbound interceptions were more representative of midday conditions (09:00 – 12:00 UTC).

https://doi.org/10.5194/egusphere-2026-3147
Preprint. Discussion started: 25 June 2026

3. Results and discussions

3.1 Overview of in-Plume and out-plume results from airborne measurements

Figure 3 compares average concentrations of PM_1 (for Flight A028, A032, and A033) or NR-PM_1 (for Flight A027(a), A027(b), A031, A034, and A036) components from the plume period with those from the nearest out-plume background period. The total PM_1 mass concentration from the airborne measurement was determined as the sum of the NR-PM_1 and rBC mass concentration measured by the mAMS and the SP2, respectively. Flights were categorized into heavy and light pollution cases based on their average PM_1 concentrations, using a threshold of 3 μg m^{-3} derived from the median PM_1 mass concentration across all flights. The term "heavy" and "light" refer to relatively higher and lower PM_1 levels within the airborne measurements, rather than representing absolute pollution categories. Among all the components, Org dominated the contribution of PM_1 mass concentrations (accounted more than 50% of total PM_1 mass concentration) across all the flights during both in-plume and out-plume periods followed by the SO_4 and pNO_3. According to the flights with available SP2 measurements, rBC contributed less than 5% to the total PM_1 mass concentration.

Compared with out-plume periods, although total PM_1 mass concentrations showed a statistical increase during in-plume periods (confirmed by t-test, $p < 0.05$), the magnitude of the increase was modest (< 2 μg m^{-3}). This was primarily due to that the regional background plays an important role in total air mass Beekmann et al. (2015) suggested that regional transport from upwind regions contribute 70% of the fine particles ($PM_{2.5}$) in Paris region on average. The Southwest (SW) Flight A027 exhibited the highest NR-PM_1 concentrations among all flights, consistent with ground-based measurements at Paris suburban site (Rambouillet forest site) (Yu et al., 2025) during the campaign. This indicated that air masses originating from the northwest increased overall pollution levels over Paris region during this flight.

Compared with previous airborne measurements over other urban regions, observations across Europe (McMeeking et al., 2012; Freney et al., 2014; Morgan et al., 2010), Asia (Nault et al., 2018), and Americas (Shingler et al., 2016; Vu et al., 2016; DeCarlo et al., 2008; Shilling et al., 2018), consistently indicate a substantial contribution of Org to total PM_1 mass within downwind urban plumes relative to regional background conditions across diverse environments. This is consistent with our findings, which show that Org contributes significantly to total PM_1 mass in the downwind plume of Paris. Previous studies over Paris (Freney et al., 2014) and London (McMeeking et al., 2012) have shown that marine-influenced air masses are typically associated with an enhanced mass fraction of SO_4. However, our measurements during marine air mass influence periods (A031 and A036) did not exhibit a significant contribution of SO_4 to total PM_1 mass concentrations. This reduced SO_4 contribution was likely attributable to decreased sulfur oxides (SO_x) emissions from shipping activities over the Atlantic Ocean, following the implementation of stricter sulfur regulations by the International Maritime Organization (IMO) in 2020. Yu et

https://doi.org/10.5194/egusphere-2026-3147
Preprint. Discussion started: 25 June 2026

al. (2020) estimated that SO_4 emissions from shipping over the Atlantic Ocean declined by more than 80%, resulting in a lower SO_4 contribution in regional air masses advected to the European urban region.

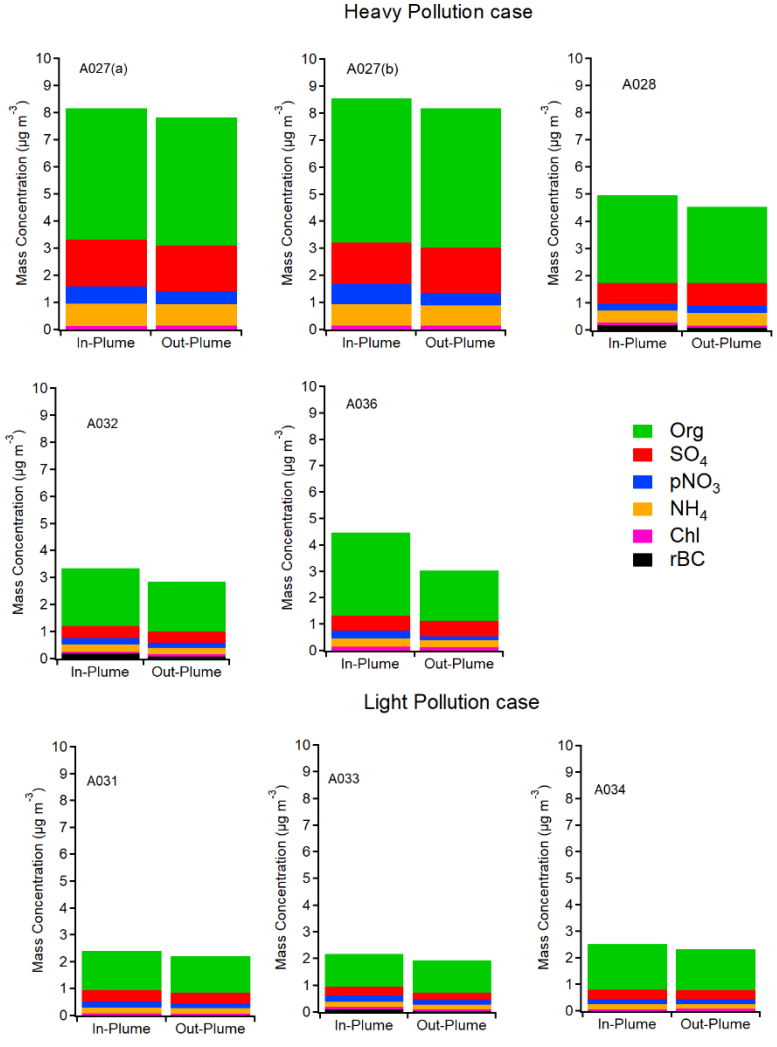

Figure 3. Comparison of PM_1 or NR-PM_1 component mass concentrations during the in-plume period and the nearest out-plume background period. rBC data from the SP2 measurements were available only for Flights A028, A032, and A033; therefore, results were reported as PM_1 for these flights and as NR-PM_1 for the remaining flights. Details of the average mass concentrations of each aerosol component, along with the standard deviation for each flight, are presented in Table S4 in the Supplementary Information.

https://doi.org/10.5194/egusphere-2026-3147
Preprint. Discussion started: 25 June 2026

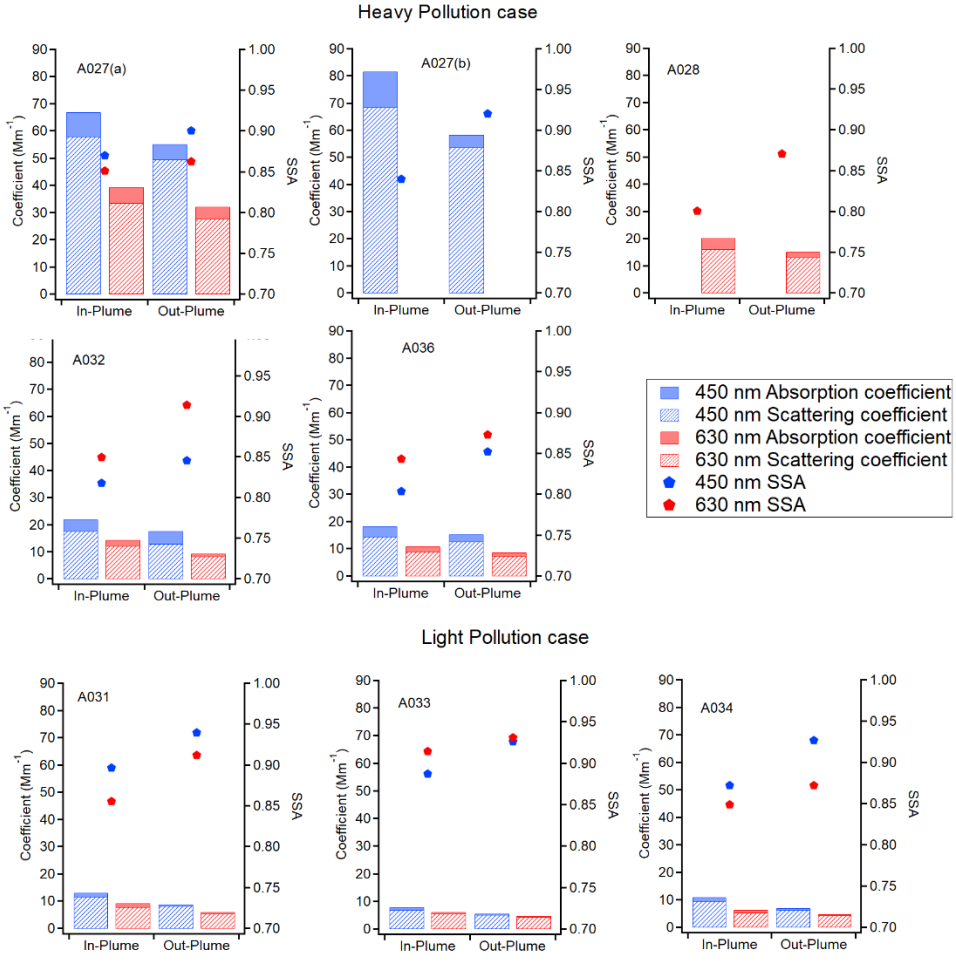

Figure 4. Comparison of average aerosol scattering and absorption coefficients at 450 and 630 nm for the in-plume period and the nearest out-plume background period. The corresponding SSA at both wavelengths is also presented for in-plume and out-plume periods. Details of the average σ_{ext}, σ_{scat}, and SSA at both 450 nm and 630 nm, along with their standard deviations for each flight, are presented in Table S5 in the Supplementary Information.

Figure 4 shows the in-plume and out-plume average aerosol scattering and absorption coefficients, along with average SSA, at 450 and 630 nm for all flights. The average in-plume σ_{ext} at 450 and 630 nm was higher than during out-plume periods due to enhanced NR-PM_1 levels (confirmed by t-test, $p < 0.05$). The average in-plume SSA was lower than the average out-plume SSA at both 450 and 630 nm indicating that the Paris urban plume generally enhanced the light-absorbing capacity of regional aerosols. Most flights exhibited lower average SSA at 450 nm than at 630 nm. Such wavelength-dependent absorption and the fact that the average SAE values derived from the airborne measurements exceeded 1 (Figure 9), suggests a potential contribution from brown carbon (BrC) that exhibited stronger absorption at shorter wavelengths (Laskin et al., 2015). However,

https://doi.org/10.5194/egusphere-2026-3147
Preprint. Discussion started: 25 June 2026

only a few flights (A027(a), A031, and A034) exhibited lower SSA at 630 nm, suggesting a potentially stronger contribution from rBC, whose absorption exhibits relatively weak spectral dependence.

Compared with previous airborne observations over urban regions, the measured σ_{ext} at 630 nm observed in this study was comparable to values observed over the Denver metropolitan area in summer under similar NR-PM_1 aerosol loading levels (σ_{ext} at 630 nm < 20 Mm^{-1} and NR-PM_1 < 10 μg m^{-3} in their study) (Dingle et al., 2016). While the measured SSA observed in this study is close to the average SSA reported within the London urban plume in summer (0.89 and 0.88 at 467 nm and 652 nm, respectively) (Davies et al., 2019), our results indicate stronger absorption at shorter wavelengths in the Paris urban plume compared to London. The average SSA at 450 nm observed in this study is comparable to the boundary-layer average SSA at 440 nm over Beijing during low aerosol loading periods, which ranged from 0.80 to 0.85 (Tian et al., 2020).

3.2 Comparison between airborne and ground-based measurements

3.2.1 Evolution of particle size distribution

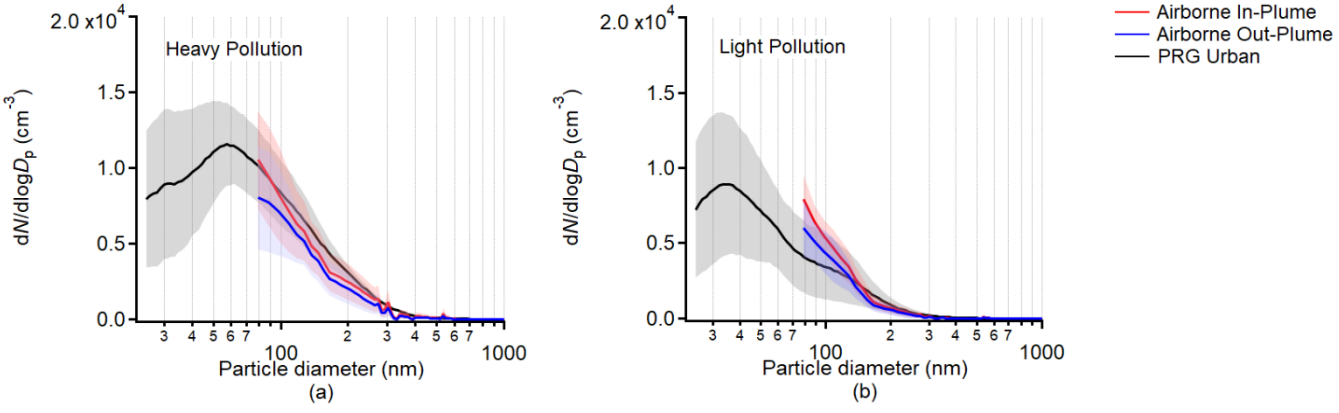

Figure 5. Average particle number size distributions measured by the PRG SMPS (fresh urban emissions) and the airborne UHSAS (in-plume and out-plume periods) during heavy (a) and light (b) pollution conditions. The shaded area indicates the uncertainty, represented by the standard deviation. PRG results were selected based on the corresponding emission time windows listed in Table S3 in the Supplementary Information.

Figure 5 compares the particle number size distributions measured at the PRG site during the estimated emission periods of the Paris urban plume with those obtained from airborne measurements during in-plume and out-plume periods downwind. During heavy-pollution periods, the particle size distributions at the PRG urban site exhibited a modal peak between 50 and 60 nm, whereas during light-pollution periods the peak shifted to smaller diameters, centred at approximately between 30 and 40 nm. Downwind aircraft measurements showed an enhancement in particle number concentrations in the 80–200 nm size

https://doi.org/10.5194/egusphere-2026-3147
Preprint. Discussion started: 25 June 2026

range during in-plume periods compared to out-plume periods. Previous studies have similarly reported that aged urban plumes exhibit enhanced particle number concentrations in this size range. Observations in urban and suburban areas of the Greater London region have shown that central urban sites exhibit higher particle number concentrations in the 30–50 nm size range, associated with fresh traffic emissions, whereas downwind suburban sites show a greater contribution at larger particle sizes (around 100–200 nm), associated with secondary aerosol components (Beddows et al., 2015; Harrison et al., 2019). Consistent with this, Cirino et al. (2018) reported enhanced particle number concentrations in the 100–200 nm size range in aged urban plumes over downwind suburban areas in South America compared to urban sites. The increase in particle number concentration in the 80–200 nm size range resulted in only a modest yet statistically increase in particle volume under in-plume conditions compared to out-plume conditions downwind of Paris (confirmed by t-test, $p < 0.05$). The average volume concentration was 5.79 (±3.34) $\mu m^3\ cm^{-3}$ for in-plume period and 4.54 (±2.43) $\mu m^3\ cm^{-3}$ for out-plume period during the heavy pollution period and was 2.47 (±0.86) $\mu m^3\ cm^{-3}$ for in-plume period and 1.93 (±0.72) $\mu m^3\ cm^{-3}$ for out-plume period during the light pollution period. This modest increase in particle volume was consistent with the PM_1 mass concentrations shown in Figure 3, which also exhibit only a limited enhancement between in-plume and out-plume periods. The size distributions at PRG and the downwind site were similar over the 80–1000 nm range. The average volume-effective radius at PRG was 308 (±34) nm (heavy pollution) and 300 (±28) nm (light pollution), compared to 318 (±63) nm and 308 (±103) nm, respectively, within the downwind plume. These differences were not statistically significant (confirmed by t-test, $p > 0.05$), indicating that volume-effective particle size remained largely unchanged within the 80–1000 nm range between the PRG site and the downwind plume.

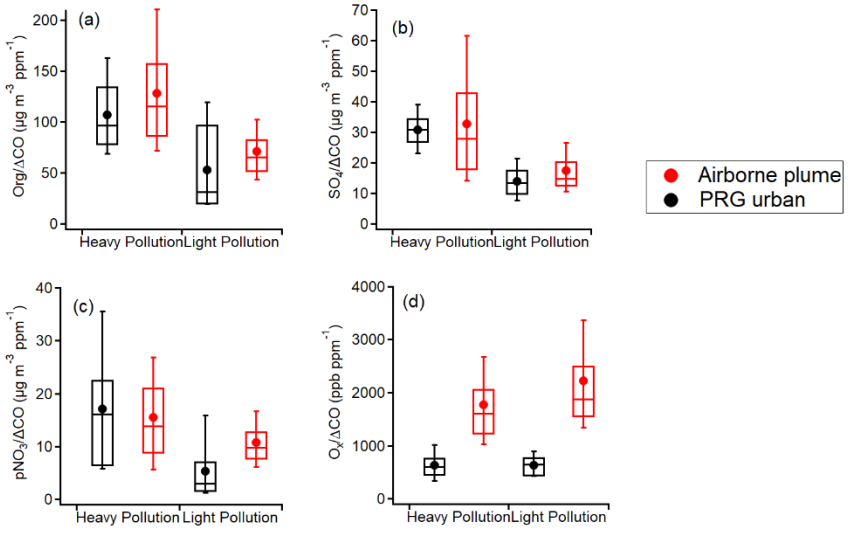

Figure 6. Concentrations of (a) organic aerosol (Org), (b) sulfate (SO_4), (c) nitrate (NO_3), and (d) O_x (NO_2 + O_3) measured at the PRG urban site and in the downwind urban plume from airborne observations during heavy and light pollution periods. Results are normalised to ΔCO to account for dilution. Boxes show the interquartile range (25th–75th percentiles), whiskers indicate the 10th–90th percentiles, the horizontal line represents the median, and the dots denote the mean values.

https://doi.org/10.5194/egusphere-2026-3147
Preprint. Discussion started: 25 June 2026

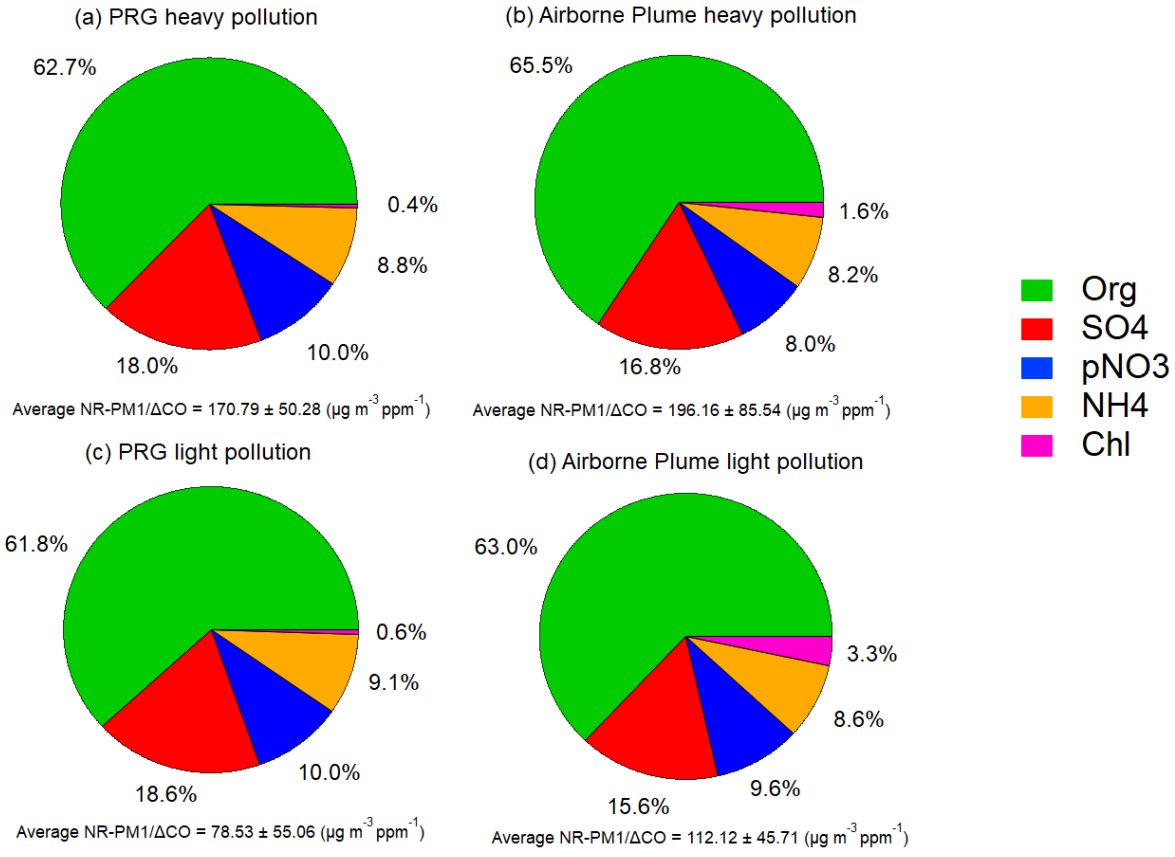

Figure 7. Mass fraction of NR-PM$_1$ components measured at (a)(c) PRG urban site and (b)(d) downwind urban plume derived from airborne results at heavy and light pollution periods. The uncertainty in the average NR-PM$_1$/ΔCO represents the standard deviation.

Figures 6 and 7 show the normalised NR-PM$_1$ component concentrations and O_x (NO_2 + O_3), as well as the mass fractions of NR-PM$_1$ components measured at the PRG urban site and in the downwind urban plume from airborne observations during heavy and light pollution periods. Results in Figure 6 are normalised to ΔCO to account for dilution. The average O_x/ΔCO was statistically similar at the PRG urban site at different pollution level (confirmed by t-test, $p > 0.05$) indicating that the initial photochemical age may be close under the different pollution level. The airborne measured downwind aged urban plume show higher average O_x/ΔCO compared to the measurements at PRG (statistically difference confirmed by t-test, $p < 0.05$), indicating that the urban plume has experienced photochemical aging process during the transport. Accordingly, the average Org/ΔCO downwind increased by around 30% under both pollution level, indicating SOA formation during the aging process. The Org mass fraction also increased in the downwind plume relative to the PRG site under both pollution regimes, indicating that SOA formation was the dominant contributor to the increase in NR-PM$_1$/ΔCO during plume aging. This agrees with studies in urban environments which demonstrated that SOA formation is the dominant driver of NR-PM$_1$ enhancement during

https://doi.org/10.5194/egusphere-2026-3147
Preprint. Discussion started: 25 June 2026

photochemical processing (Yu et al., 2025; Wu et al., 2022; Hayes et al., 2013; Chen et al., 2021; Dingle et al., 2016; DeCarlo et al., 2010; Nault et al., 2018). $SO_4/\Delta CO$ did not show a statistically significant difference between the PRG site and the downwind Paris urban plume across different pollution regimes (statistically similar confirmed by t-test, $p > 0.05$). This may be due to limited precursor availability within the urban plume, as SO_x emissions have declined across European urban areas over the past decades (Ciarelli et al., 2019; Tsimpidi et al., 2025). While the $pNO_3/\Delta CO$ presented a statistical increase trend after the plume aging process during light pollution period (confirmed by t-test, $p < 0.05$), there was no statistically significant change observed during the heavy pollution period (statistically similar confirmed by t-test, $p > 0.05$). A possible reason may be the substantial background contribution of pNO_3 during the heavy pollution period, which may mask relatively small enhancements associated with the urban plume. Such variations may become more apparent during the light pollution period. Another possibility is the enhanced evaporation of pNO3 to the gas phase during aging under heavy pollution conditions, when temperatures were higher than during the light pollution period. The average temperature measured onboard the aircraft was higher during the heavy pollution periods (18.2 ± 1.6 °C) compared to the light pollution periods (15.7 ± 1.7 °C) (statistically different confirmed by t-test, $p < 0.05$). Although the average RH measured onboard the aircraft was also higher during the heavy pollution period ($58 \pm 11\%$) than during the light pollution period ($52 \pm 5\%$) (statistically different confirmed by t-test, $p < 0.05$), the higher temperatures likely played a key role in promoting the volatilization of ammonium nitrate, thereby reducing pNO_3 formation efficiency. This is similar to prior airborne studies, such as DeCarlo et al. (2008), that observed decreases of pNO_3 as the urban plume over Mexico City was transported away from the city core.

https://doi.org/10.5194/egusphere-2026-3147
Preprint. Discussion started: 25 June 2026

3.3 Impacts of plume aging on aerosol optical properties

3.3.1 Evolution of CRI and SSA

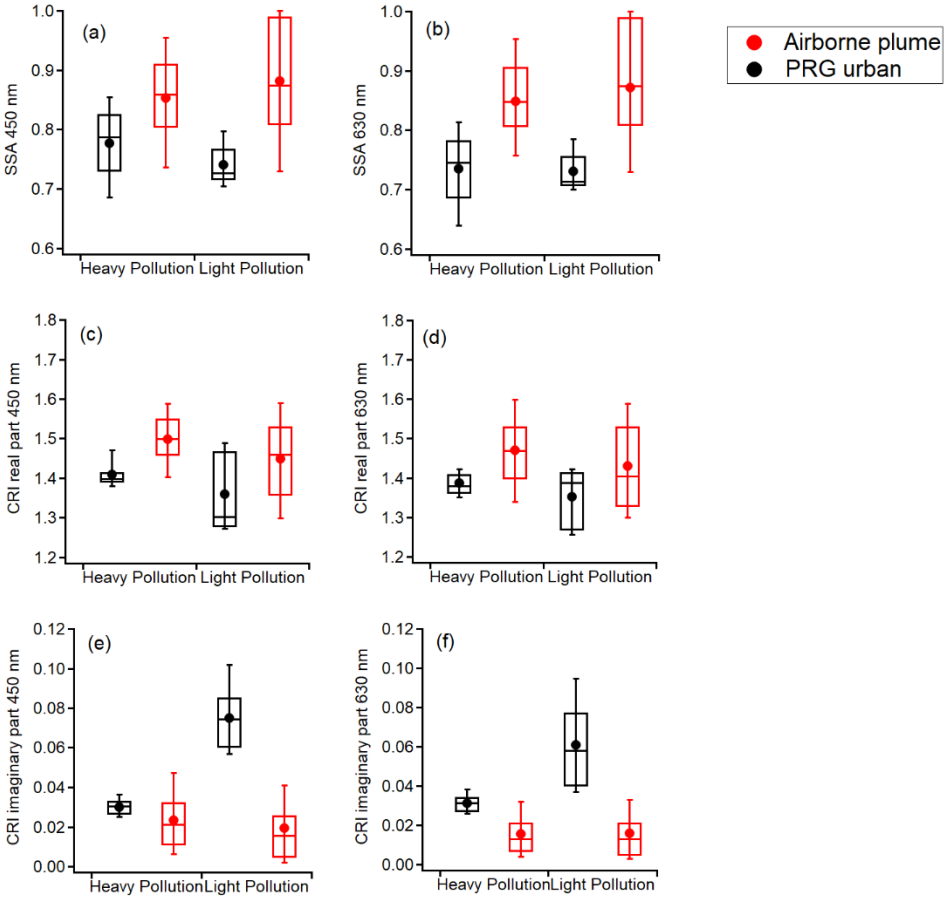

Figure 8. SSA at (a) 450 nm and (b) 630 nm, and complex refractive index (CRI) at (c, d) the real part and (e, f) the imaginary part at 450 nm and 630 nm, respectively. Results are shown for PRG site measurements and airborne observations during heavy and light pollution periods. Boxes show the interquartile range (25th–75th percentiles), whiskers indicate the 10th–90th percentiles, the horizontal line represents the median, and the dots denote the mean values.

Figure 8 presents the comparison between the SSA and CRI in fresh urban plume from the PRG urban measurements and the aged plume measured by the aircraft at different pollution levels. Downwind Paris urban plume, the light pollution-plumes average SSA was statistically higher than that observed during heavy pollution periods in the airborne measurements (confirmed by t-test $p < 0.05$), reflecting a relatively weaker contribution from absorbing components (Figure 8(a)(b)).

https://doi.org/10.5194/egusphere-2026-3147
Preprint. Discussion started: 25 June 2026

At the PRG site, no statistically significant difference was observed in the average SSA at 630 nm between pollution regimes (confirmed by t-test, $p > 0.05$, Figure 8(b)), whereas the average SSA at 450 nm was slightly lower during light pollution periods (statistically different confirmed by t-test, $p < 0.05$, Figure 8(a)). Consistent with this behaviour, the imaginary part of the CRI increased at both wavelengths during light pollution periods compared to heavily polluted periods (Figure 8(e)(f)). This is likely due to the proximity of the PRG site to emission sources and the inclusion of morning rush-hour emissions (04:00–08:00 UTC) in the selected plume emission period, in agreement with the diurnal analysis presented in Di Antonio et al. (2025). Meanwhile, during periods of light pollution, the reduced influence of regionally transported NR-PM_1 enhanced the relative contribution from local traffic emissions, resulting in an increase in the imaginary part of the CRI at the PRG site despite overall cleaner conditions. In contrast, airborne measurements downwind did not show the same trend in the imaginary part of the CRI. While the real part of the CRI during the light pollution periods was lower than that observed during heavy pollution periods downwind of the Paris urban plume (statistically different confirmed by t-test, $p < 0.05$, Figure 8(c)(d)), the imaginary part remained statistically similar (confirmed by t-test, $p > 0.05$, Figure 8(e)(f)). This suggests that the variation in the imaginary part of the CRI at the PRG site during light-pollution periods was likely driven by local sources.

The average SSA showed differences between measurements at the PRG site and the downwind aged plume. At both 450 and 630 nm, the average SSA increased from below 0.8 in the fresh urban emissions at PRG to above 0.8 in the aged Paris urban plume from the aircraft measurements (Figure 8(a)(b)). This increase in SSA indicates a transition of the aerosol population from a more absorption-dominated regime toward a more scattering-dominated one. This variation of SSA is consistent with previous airborne measurements downwind of Los Angeles (Langridge et al., 2012) and London (Mcmeeking et al., 2012), which also report a progressive transition toward more scattering-dominated aerosol populations. Consistent with the SSA evolution, the average CRI also changed between fresh and aged plume conditions. At PRG, the average real part of the CRI was approximately 1.35 to 1.4 (Figure 8(c)(d)), while the average imaginary part ranged from 0.03 to 0.08 at both 450 and 630 nm (Figure 8(e)(f)). In contrast, airborne measurements of the aged plume showed a higher average real part (~1.45–1.50, Figure 8(c)(d)) together with a lower average imaginary part (~0.015–0.02, Figure 8(e)(f)) at both wavelengths (statistically different confirmed by t-test $p < 0.05$).

These variations in SSA and CRI may be driven by changes in aerosol chemical composition during plume aging. In particular, the decrease in the imaginary part of the CRI at both wavelengths suggests a reduced relative contribution from strongly absorbing particles. As presented in Figure S2 in the Supplementary Information, for flights with SP2 measurements available, the rBC mass fraction decreased downwind of the urban plume during both heavy and light pollution periods. This decrease of rBC mass fraction was more pronounced during the light pollution period, consistent with the larger reduction in the imaginary part observed under these conditions. Observations across diverse environments globally have shown that a reduction in BC mass fraction leads to an increase in SSA at both short and long wavelengths. (Eom et al., 2025). Ground-based measurements during the ACROSS project period also indicate that the imaginary part of the CRI was strongly

https://doi.org/10.5194/egusphere-2026-3147
Preprint. Discussion started: 25 June 2026

associated with BC (reported as eBC in that study) mass fraction, and its reduction at the downwind suburban forest sites led to a lower imaginary part compared to the PRG site (Di Antonio et al., 2025). Meanwhile, given the substantial contribution of Org to NR-PM_1 at both PRG site and downwind urban plume, the increase in the real part of the bulk aerosol CRI may be largely driven by changes in the optical properties of Org during plume aging. As shown in the supplementary, estimates based on measured NR-PM_1 species mass concentrations indicate that the average real part of the Org CRI increased from fresh urban emissions at the PRG site to the more aged urban plume sampled downwind during the airborne measurements. Similar behaviour has been reported in previous studies. Shen et al. (2025) reported that an increasing fraction of SOA within total Org may lead to an increase in the average real part of the Org CRI in the urban environment. Flores et al. (2014) also observed an increase in the real part of the CRI during laboratory photooxidation of mixed biogenic and anthropogenic VOCs. In their experiments, the real part of the CRI increased from ~1.46 to ~1.51 at 405 nm after a photochemical aging within 4h. As Org contributes substantially to NR-PM_1, the higher real part of the CRI associated with photo-oxidized Org may drive the increase in the population-averaged CRI real part downwind of the urban plume.

3.3.2 Evolution of the wavelength dependence of aerosol optical properties

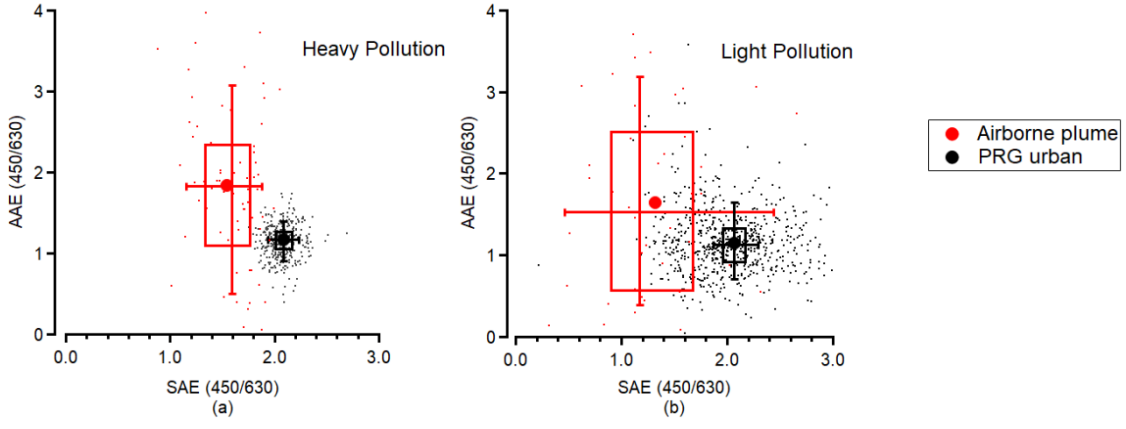

Figure 9. AAE versus SAE for the airborne-measured Paris urban plume and the corresponding ground-based measurements at the PRG site at (a) heavy pollution period and (b) light pollution period. Boxes show the interquartile range (25th–75th percentiles), whiskers indicate the 10th–90th percentiles, the horizontal line represents the median, and the dots denote the mean values.

Figure 9 compares the AAE and SAE derived from airborne and PRG ground-based measurements. Owing to the lower aerosol concentrations in the airborne observations, these results exhibited larger variability compared to the PRG urban measurements. Therefore, the impact of differing measurement size cutoffs was likely minor. The spectral dependence of both absorption and scattering evolved with plume aging. As shown in Figure 9, the average AAE at the PRG site was close to 1, and the average SAE was approximately 2 at both pollution levels, with no statistically significant differences between regimes (confirmed by t-test, $p > 0.05$). Similarly, airborne measurements within the plume showed comparable values at both pollution levels, with

https://doi.org/10.5194/egusphere-2026-3147
Preprint. Discussion started: 25 June 2026

average AAE close to 2 and average SAE around 1.5, and no statistically significant differences observed (confirmed by t-test, $p > 0.05$).

During downwind evolution and dilution of the Paris urban plume, the airborne observations downwind the Paris urban plume show increasing average AAE and decreasing average SAE at both pollution levels compared to the Paris urban measurements (statistically different confirmed by t-test, $p < 0.05$). Several factors likely contributed to the observed changes in the spectral dependence of both aerosol absorption and scattering during plume aging. The reduction in rBC mass fraction downwind of the Paris urban plume led to a fractional decrease in its contribution to total light absorption compared to PRG site. Meanwhile, elevated Org/ΔCO during urban plume transport indicate enhanced SOA formation, which may favour the production of BrC. While overall aerosol absorption weakened during plume aging, the fractional contribution of BrC increased. The average BrC absorption fraction increased from 15.7 (±17.7) % and 8.9 (±6.9) % under heavy and light pollution conditions at the PRG site to 39.1 (±20.8) % and 42.0 (±31.1) %, respectively, within the downwind plume. This enhanced BrC contribution shifted the spectral absorption toward shorter wavelengths, resulting in higher average AAE in the downwind plume. This interpretation is consistent with measurements on the ground during the ACROSS campaign period (Yu et al., 2025), which reports an increase of BrC absorption fraction at short wavelength to summertime light absorption associated with active secondary processes. Similar trend was also observed in the comparison between Paris urban site and suburban sites in Di Antonio et al. (2025). During the campaign, the downwind suburban sites had relatively higher BrC absorption fraction compared to the Paris urban site. The observed decrease in average SAE may partially attributed to differences in the upper size cutoffs used in the airborne (10 μm) and ground-based PRG (1 μm) measurements. However, the influence of coarse mode particles was expected to be limited, as indicated by the consistently high average SAE values (>1). Furthermore, although the volume-effective particle size showed little variation within the 80–1000 nm range between the PRG site and the downwind plume, indicating limited particle growth within this size range, potential size-resolved compositional changes (Zaveri et al., 2010) cannot be excluded and may have contributed to the observed decrease in average SAE.

https://doi.org/10.5194/egusphere-2026-3147
Preprint. Discussion started: 25 June 2026

3.3.3 Comparison of CRI at the urban site and downwind with previous measurements

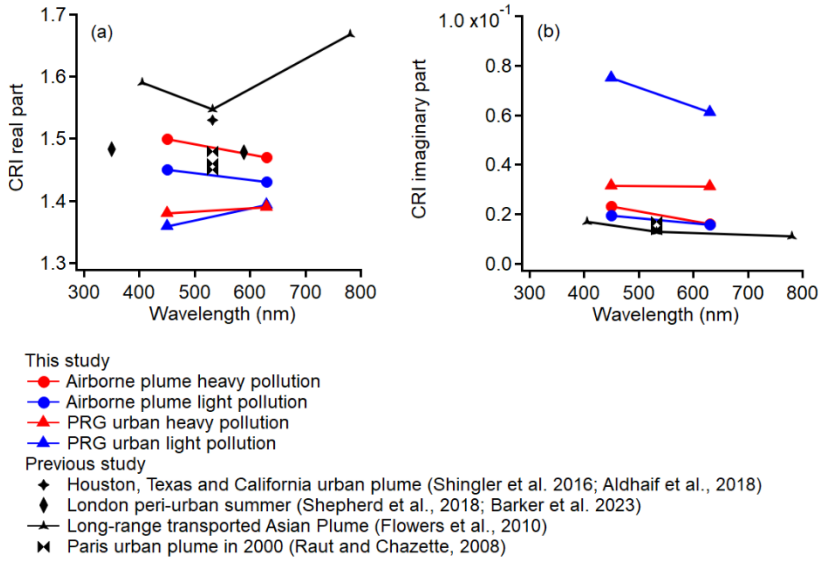

Figure 10. Comparison of CRI (a) real part and (b) imaginary part derived from this study and other urban plume characterisation studies (Shingler et al., 2016; Aldhaif et al., 2018; Shepherd et al., 2018; Barker et al., 2023; Flowers et al., 2010; Raut and Chazette, 2008).

Figure 10 compares the average CRI measured in this study with values reported in previous urban plume characterisation studies. Our results suggest that aerosols in urban environments dominated by primary emissions exhibit lower real and higher imaginary parts of the CRI, whereas downwind regions with stronger secondary contributions show the opposite pattern. A similar trend has also been observed in urban areas in China, where lower CRI real part values of NR-PM_1 are associated with stronger primary emissions, whereas higher values are linked to greater secondary components contributions (Wu et al., 2021; Shen et al., 2025).

The real part of the CRI measured in London during summer is comparable to the aircraft observations downwind Paris urban plume but higher than the PRG urban measurements, which may reflect the peri-urban nature of the sampling locations and the influence of more aged urban plumes in their study (Shepherd et al., 2018). Both the real and imaginary parts of the CRI observed in our study are slightly higher than those reported by airborne measurements conducted closer to the Paris region in 2000 (Raut and Chazette, 2008). This difference is likely due to the more aged aerosols in our study, which again is consistent with our observed changes with plume age. The real part of the CRI observed downwind of American megacities is higher than that measured in this study, likely due to a larger contribution from secondary inorganic components with higher CRI real part in their observations (Aldhaif et al., 2018; Shingler et al., 2016). Flowers et al. (2010) reports CRI values for long-range transported Asian plumes measured at a remote site, which exhibit a higher real part and a lower imaginary part than those

https://doi.org/10.5194/egusphere-2026-3147
Preprint. Discussion started: 25 June 2026

observed in the relatively early aged urban plumes investigated here and in previous studies. These comparison results highlight the dynamic nature of the CRI, which evolves with aerosol composition and chemical aging. Consequently, assuming a static CRI for either bulk aerosol or individual components, particularly the Org fraction, represents an oversimplification and may introduce uncertainties in model simulations or satellite retrievals (Levy et al., 2007; Herrera et al., 2022; Curci et al., 2019). A dynamic parametrization that accounts for atmospheric processing (e.g. (Konovalov et al., 2021; Drugé et al., 2022; Jiang et al., 2024)) would therefore provide a more realistic representation of aerosol optical properties.

Conclusions

In this study, we analysed results from an airborne and a ground-based measurement campaign over the Paris region to characterise the evolution of the physicochemical and optical properties of the urban plume after approximately 2–6 hours of atmospheric aging. Measurements show that the Paris urban plume is an important source of very fine particles (80–200 nm size range). The downwind Paris urban plume exhibited a net production of NR-PM_1 relative to primary emissions, primarily driven by an increased contribution of organic matter (Org), in agreement with previous research in similar environments (Nault et al., 2018; Freney et al., 2014; DeCarlo et al., 2008). In contrast, secondary inorganic species showed limited variation during plume aging and contributed a smaller fraction of PM_1 compared to previous European airborne studies of urban plumes (McMeeking et al., 2012; Freney et al., 2014), reflecting recent changes in anthropogenic pollutant emissions in European urban regions (Yu et al., 2020; Tsimpidi et al., 2025; Ciarelli et al., 2019). The plume aging led to a more scattering-dominated aerosol population. The average SSA downwind the Paris urban plume increased at both 450 and 630 nm, consistently with the increase in the real part of the CRI ~1.35–1.40 at the PRG site to ~1.45–1.50 in the aged urban plume downwind, indicating enhanced light scattering, while the imaginary part decreased from ~0.03–0.08 to ~0.015–0.02, reflecting a reduced contribution to light absorption. The CRI measured downwind of the Paris urban plume falls within the range reported for downwind urban plumes and suburban regions (Shingler et al., 2016; Aldhaif et al., 2018; Shepherd et al., 2018; Barker et al., 2023; Raut and Chazette, 2008). The evolution of aerosol optical properties during plume aging was associated with a reduced fractional contribution of rBC to light absorption, as indicated by a decrease in rBC mass fraction and an increase in AAE, consistent with previous studies linking lower BC mass fractions to more scattering-dominated aerosols (Di Antonio et al., 2025; Eom et al., 2025). The increase in average AAE in the downwind urban plume indicates a greater fractional contribution of BrC to short-wavelength absorption; however, this increase appears insufficient to offset the overall decrease in absorption and the concurrent increase in scattering. The observed decrease in average SAE in the downwind Paris urban plume suggested a larger relative contribution of larger particles to scattering, potentially due to differences in size cutoffs on different measurement platform and/or size-resolved compositional changes. Incorporating size-resolved compositional observations in future work could help further investigate how compositional evolution across different particle sizes influences the observed optical properties.

https://doi.org/10.5194/egusphere-2026-3147
Preprint. Discussion started: 25 June 2026

In summary, our results demonstrate a clear evolution of aerosol physicochemical and optical properties within the urban plume, driven by a shift from more primary-emission-impacted to more secondary-process-impacted conditions. Such differences may not be fully represented in some atmospheric models and satellite retrieval algorithms that rely on fixed CRI values and simplified aerosol optical assumptions. While recent model and satellite retrieval studies (e.g. (Drugé et al., 2022; Jiang et al., 2024)) have introduced dynamic parameterizations to account for atmospheric processing of aerosol optical properties, substantial uncertainties remain in key optical parameters such as SSA (Li et al., 2022a). In-situ measurements are therefore essential to provide observational constraints, particularly in the context of recent changes in global anthropogenic emissions (Li et al., 2023). To the best of our knowledge, this study represents one of the few post-2017 airborne investigations of aerosol physicochemical properties over a European megacity. The derived CRI, together with the observed SSA, offers valuable constraints for improving the representation of aerosol optical properties in chemical transport models and remote-sensing retrievals.

Data availability

Processed ACROSS flight campaign data are archived at ACROSS AERIS: https://across.aeris-data.fr/ (last accessed 21/03/2026). AIRPARIF data is available from: https://www.airparif.fr/ (last access 11/12/2025).

Author Contributions

CC, PF and VM designed the ACROSS-AO aircraft campaign. CY and PFD operated the mAMS instrument on board the ATR-42 aircraft and performed the associated data analysis, together with BAN. CY conducted the A2S2 measurements on board the ATR-42 and performed the associated data analysis. EA and PDC operated the TD-LIF instrument on the ATR-42 aircraft and performed the associated the data analysis. CD, ST, and TB operated the SP2 instrument on board the ATR-42 aircraft and AVG performed the data analysis. EP, KT, MC, NG, and TB contributed to the modification and configuration of instruments on board the ATR-42 aircraft. DLP, KT, AB, CC, and VM contributed to the airborne experiment. LDA, CDB, AG, AB, BDA and JK conducted the PRG experiment and analysed the data. CY and HW performed the NAME back trajectory analysis. LDA, MB, GS, and GF provided meteorological and chemical forecast for the flight campaign. CY and PF led the data analysis and drafted the manuscript. All co-authors contributed to the interpretation of the results and provided comments on the manuscript.

Acknowledgment

Airborne data was obtained using the aircraft managed by Safire, the French facility for airborne research, an infrastructure of the French National Center for Scientific Research (CNRS), Météo-France and the French National Center for Space Studies (CNES). The authors wish to thank AERIS (https://www.aeris-data.fr/, last access: 11/12/2025), the French centre for atmospheric data and service, for providing the campaign website and organizing the curation and open distribution of the ACROSS data. Chenjie Yu would like to acknowledge the Marie Skłodowska-Curie COFUND Paris Regional Postdoctoral

Fellowship program supported by the Paris Region. The participation of Peter F. DeCarlo to the ACROSS field campaign was funded by the Invited Professor program of the Université Paris Est Créteil. A. Velazquez Garcia's work is supported by the ANR (ANR-20-CE01-0010 and ANR-24-CE01-3132) and Météo-France. Contributions to the PRG set up and measurements by S. Chevaillier, C. Gaimoz, A. Feron. P. Zapf, F. Maisonneuve, G. Močnik, O. Favez, L. Hawkins, S. Riley, and D. Pronovost are gratefully acknowledged. The ACROSS Forecasting team (LISA, SAFIRE, Météo-France) is acknowledged for providing meteorological and chemical forecast supporting the choices of specific predefined flight paths. Special thanks to James D. Allan (University of Manchester) for the valuable discussions and suggestions contributing to this study.

Financial support

Airborne measurements using the Safire ATR-42 aircraft were supported by the ACROSS project, which benefits from French state aid (ANR – "Investissements d'avenir"); References: ANR-17-MPGA-0002 and ANR-20-CE01-0010. Measurements conducted at PRG site was supported by the French National program LEFE (Les Enveloppes Fluides et l'Environnement) of the CNRS/INSU (Centre National de la Recherche Scientifique/Institut National des Sciences de L'Univers) in the framework of ACROSS-GO project. This research also receives funding from the European Union's Horizon 2020 research and innovation programme under the Marie Skłodowska-Curie grant agreement n° 945298.

Reference

Aldhaif, A. M., Stahl, C., Braun, R. A., Moghaddam, M. A., Shingler, T., Crosbie, E., Sawamura, P., Dadashazar, H., Ziemba, L., Jimenez, J. L., Campuzano-Jost, P., and Sorooshian, A.: Characterization of the Real Part of Dry Aerosol Refractive Index Over North America From the Surface to 12 km, Journal of Geophysical Research: Atmospheres, 123, 8283–8300, https://doi.org/10.1029/2018JD028504, 2018.

Barker, C. R., Poole, M. L., Wilkinson, M., Morison, J., Wilson, A., Little, G., Stuckey, E. J., Welbourn, R. J. L., Ward, A. D., and King, M. D.: Ultraviolet refractive index values of organic aerosol extracted from deciduous forestry, urban and marine environments, Environmental Science: Atmospheres, 3, 1008–1024, 10.1039/D3EA00005B, 2023.

Baron, P. A. and Willeke, K.: Aerosol Measurement: Principles, Techniques, and Applications: Second Edition [2001], John Wiley and Sons2001.

Beddows, D. C. S., Harrison, R. M., Green, D. C., and Fuller, G. W.: Receptor modelling of both particle composition and size distribution from a background site in London, UK, Atmos. Chem. Phys., 15, 10107–10125, 10.5194/acp-15-10107-2015, 2015.

Beekmann, M., Prévôt, A. S. H., Drewnick, F., Sciare, J., Pandis, S. N., Denier van der Gon, H. A. C., Crippa, M., Freutel, F., Poulain, L., Ghersi, V., Rodriguez, E., Beirle, S., Zotter, P., von der Weiden-Reinmüller, S. L., Bressi, M., Fountoukis, C., Petetin, H., Szidat, S., Schneider, J., Rosso, A., El Haddad, I., Megaritis, A., Zhang, Q. J., Michoud, V., Slowik, J. G., Moukhtar, S., Kolmonen, P., Stohl, A., Eckhardt, S., Borbon, A., Gros, V., Marchand, N., Jaffrezo, J. L., Schwarzenboeck, A., Colomb, A., Wiedensohler, A., Borrmann, S., Lawrence, M., Baklanov, A., and Baltensperger, U.: In situ, satellite measurement and model evidence on the dominant regional contribution to fine particulate matter levels in the Paris megacity, Atmos. Chem. Phys., 15, 9577–9591, 10.5194/acp-15-9577-2015, 2015.

Bond, T. C., Doherty, S. J., Fahey, D. W., Forster, P. M., Berntsen, T., DeAngelo, B. J., Flanner, M. G., Ghan, S., Kärcher, B., Koch, D., Kinne, S., Kondo, Y., Quinn, P. K., Sarofim, M. C., Schultz, M. G., Schulz, M., Venkataraman, C., Zhang, H., Zhang, S., Bellouin, N., Guttikunda, S. K., Hopke, P. K., Jacobson, M. Z., Kaiser, J. W., Klimont, Z., Lohmann, U., Schwarz, J. P., Shindell, D., Storelvmo, T., Warren, S. G., and Zender, C. S.: Bounding the role of black carbon in the climate system:

https://doi.org/10.5194/egusphere-2026-3147
Preprint. Discussion started: 25 June 2026

A scientific assessment, Journal of Geophysical Research: Atmospheres, 118, 5380–5552, https://doi.org/10.1002/jgrd.50171, 2013.

Brown, H., Liu, X., Pokhrel, R., Murphy, S., Lu, Z., Saleh, R., Mielonen, T., Kokkola, H., Bergman, T., Myhre, G., Skeie, R. B., Watson-Paris, D., Stier, P., Johnson, B., Bellouin, N., Schulz, M., Vakkari, V., Beukes, J. P., van Zyl, P. G., Liu, S., and Chand, D.: Biomass burning aerosols in most climate models are too absorbing, Nature Communications, 12, 277, 10.1038/s41467-020-20482-9, 2021.

Cantrell, C. and Michoud, V.: An Experiment to Study Atmospheric Oxidation Chemistry and Physics of Mixed Anthropogenic–Biogenic Air Masses in the Greater Paris Area, Bulletin of the American Meteorological Society, 103, 599–603, https://doi.org/10.1175/BAMS-D-21-0115.1, 2022.

Capes, G., Johnson, B., McFiggans, G., Williams, P. I., Haywood, J., and Coe, H.: Aging of biomass burning aerosols over West Africa: Aircraft measurements of chemical composition, microphysical properties, and emission ratios, Journal of Geophysical Research: Atmospheres, 113, https://doi.org/10.1029/2008JD009845, 2008.

Chen, G., Canonaco, F., Tobler, A., Aas, W., Alastuey, A., Allan, J., Atabakhsh, S., Aurela, M., Baltensperger, U., Bougiatioti, A., De Brito, J. F., Ceburnis, D., Chazeau, B., Chebaicheb, H., Daellenbach, K. R., Ehn, M., El Haddad, I., Eleftheriadis, K., Favez, O., Flentje, H., Font, A., Fossum, K., Freney, E., Gini, M., Green, D. C., Heikkinen, L., Herrmann, H., Kalogridis, A.-C., Keernik, H., Lhotka, R., Lin, C., Lunder, C., Maasikmets, M., Manousakas, M. I., Marchand, N., Marin, C., Marmureanu, L., Mihalopoulos, N., Močnik, G., Nęcki, J., O'Dowd, C., Ovadnevaite, J., Peter, T., Petit, J.-E., Pikridas, M., Matthew Platt, S., Pokorná, P., Poulain, L., Priestman, M., Riffault, V., Rinaldi, M., Różański, K., Schwarz, J., Sciare, J., Simon, L., Skiba, A., Slowik, J. G., Sosedova, Y., Stavroulas, I., Styszko, K., Teinemaa, E., Timonen, H., Tremper, A., Vasilescu, J., Via, M., Vodička, P., Wiedensohler, A., Zografou, O., Cruz Minguillón, M., and Prévôt, A. S. H.: European aerosol phenomenology − 8: Harmonised source apportionment of organic aerosol using 22 Year-long ACSM/AMS datasets, Environment International, 166, 107325, https://doi.org/10.1016/j.envint.2022.107325, 2022.

Chen, T., Liu, J., Ma, Q., Chu, B., Zhang, P., Ma, J., Liu, Y., Zhong, C., Liu, P., Wang, Y., Mu, Y., and He, H.: Measurement report: Effects of photochemical aging on the formation and evolution of summertime secondary aerosol in Beijing, Atmos. Chem. Phys., 21, 1341–1356, 10.5194/acp-21-1341-2021, 2021.

Chen, Y., Xu, L., Humphry, T., Hettiyadura, A. P. S., Ovadnevaite, J., Huang, S., Poulain, L., Schroder, J. C., Campuzano-Jost, P., Jimenez, J. L., Herrmann, H., O'Dowd, C., Stone, E. A., and Ng, N. L.: Response of the Aerodyne Aerosol Mass Spectrometer to Inorganic Sulfates and Organosulfur Compounds: Applications in Field and Laboratory Measurements, Environmental Science & Technology, 53, 5176–5186, 10.1021/acs.est.9b00884, 2019.

Ciarelli, G., Theobald, M. R., Vivanco, M. G., Beekmann, M., Aas, W., Andersson, C., Bergström, R., Manders-Groot, A., Couvidat, F., Mircea, M., Tsyro, S., Fagerli, H., Mar, K., Raffort, V., Roustan, Y., Pay, M. T., Schaap, M., Kranenburg, R., Adani, M., Briganti, G., Cappelletti, A., D'Isidoro, M., Cuvelier, C., Cholakian, A., Bessagnet, B., Wind, P., and Colette, A.: Trends of inorganic and organic aerosols and precursor gases in Europe: insights from the EURODELTA multi-model experiment over the 1990–2010 period, Geosci. Model Dev., 12, 4923–4954, 10.5194/gmd-12-4923-2019, 2019.

Cirino, G., Brito, J., Barbosa, H. M. J., Rizzo, L. V., Tunved, P., de Sá, S. S., Jimenez, J. L., Palm, B. B., Carbone, S., Lavric, J. V., Souza, R. A. F., Wolff, S., Walter, D., Tota, J., Oliveira, M. B. L., Martin, S. T., and Artaxo, P.: Observations of Manaus urban plume evolution and interaction with biogenic emissions in GoAmazon 2014/5, Atmospheric Environment, 191, 513–524, https://doi.org/10.1016/j.atmosenv.2018.08.031, 2018.

Cross, E. S., Slowik, J. G., Davidovits, P., Allan, J. D., Worsnop, D. R., Jayne, J. T., Lewis †, D. K., Canagaratna, M., and Onasch, T. B.: Laboratory and Ambient Particle Density Determinations using Light Scattering in Conjunction with Aerosol Mass Spectrometry, Aerosol Science and Technology, 41, 343–359, 10.1080/02786820701199736, 2007.

Curci, G., Alyuz, U., Barò, R., Bianconi, R., Bieser, J., Christensen, J. H., Colette, A., Farrow, A., Francis, X., Jiménez-Guerrero, P., Im, U., Liu, P., Manders, A., Palacios-Peña, L., Prank, M., Pozzoli, L., Sokhi, R., Solazzo, E., Tuccella, P., Unal, A., Vivanco, M. G., Hogrefe, C., and Galmarini, S.: Modelling black carbon absorption of solar radiation: combining external and internal mixing assumptions, Atmos. Chem. Phys., 19, 181–204, 10.5194/acp-19-181-2019, 2019.

Davies, N. W., Fox, C., Szpek, K., Cotterell, M. I., Taylor, J. W., Allan, J. D., Williams, P. I., Trembath, J., Haywood, J. M., and Langridge, J. M.: Evaluating biases in filter-based aerosol absorption measurements using photoacoustic spectroscopy, Atmos. Meas. Tech., 12, 3417–3434, 10.5194/amt-12-3417-2019, 2019.

DeCarlo, P. F., Ulbrich, I. M., Crounse, J., de Foy, B., Dunlea, E. J., Aiken, A. C., Knapp, D., Weinheimer, A. J., Campos, T., Wennberg, P. O., and Jimenez, J. L.: Investigation of the sources and processing of organic aerosol over the Central Mexican

https://doi.org/10.5194/egusphere-2026-3147
Preprint. Discussion started: 25 June 2026

Plateau from aircraft measurements during MILAGRO, Atmos. Chem. Phys., 10, 5257–5280, 10.5194/acp-10-5257-2010, 2010.
DeCarlo, P. F., Dunlea, E. J., Kimmel, J. R., Aiken, A. C., Sueper, D., Crounse, J., Wennberg, P. O., Emmons, L., Shinozuka, Y., Clarke, A., Zhou, J., Tomlinson, J., Collins, D. R., Knapp, D., Weinheimer, A. J., Montzka, D. D., Campos, T., and Jimenez, J. L.: Fast airborne aerosol size and chemistry measurements above Mexico City and Central Mexico during the MILAGRO campaign, Atmos. Chem. Phys., 8, 4027–4048, 10.5194/acp-8-4027-2008, 2008.
Di Antonio, L., Di Biagio, C., Formenti, P., Gratien, A., Michoud, V., Cantrell, C., Bauville, A., Bergé, A., Cazaunau, M., Chevaillier, S., Cirtog, M., Coll, P., D'Anna, B., de Brito, J. F., De Haan, D. O., Dignum, J. R., Deshmukh, S., Favez, O., Flaud, P. M., Gaimoz, C., Hawkins, L. N., Kammer, J., Language, B., Maisonneuve, F., Močnik, G., Perraudin, E., Petit, J. E., Acharja, P., Poulain, L., Pouyes, P., Pronovost, E. D., Riffault, V., Roundtree, K. I., Shahin, M., Siour, G., Villenave, E., Zapf, P., Foret, G., Doussin, J. F., and Beekmann, M.: Aerosol spectral optical properties in the Paris urban area and its peri-urban and forested surroundings during summer 2022 from ACROSS surface observations, Atmos. Chem. Phys., 25, 3161–3189, 10.5194/acp-25-3161-2025, 2025.
Di Carlo, P., Aruffo, E., Busilacchio, M., Giammaria, F., Dari-Salisburgo, C., Biancofiore, F., Visconti, G., Lee, J., Moller, S., Reeves, C. E., Bauguitte, S., Forster, G., Jones, R. L., and Ouyang, B.: Aircraft based four-channel thermal dissociation laser induced fluorescence instrument for simultaneous measurements of NO₂, total peroxy nitrate, total alkyl nitrate, and HNO₃, Atmos. Meas. Tech., 6, 971–980, 10.5194/amt-6-971-2013, 2013.
Dingle, J. H., Vu, K., Bahreini, R., Apel, E. C., Campos, T. L., Flocke, F., Fried, A., Herndon, S., Hills, A. J., Hornbrook, R. S., Huey, G., Kaser, L., Montzka, D. D., Nowak, J. B., Reeves, M., Richter, D., Roscioli, J. R., Shertz, S., Stell, M., Tanner, D., Tyndall, G., Walega, J., Weibring, P., and Weinheimer, A.: Aerosol optical extinction during the Front Range Air Pollution and Photochemistry Experiment (FRAPPÉ) 2014 summertime field campaign, Colorado, USA, Atmos. Chem. Phys., 16, 11207–11217, 10.5194/acp-16-11207-2016, 2016.
Drewnick, F., Hings, S. S., DeCarlo, P., Jayne, J. T., Gonin, M., Fuhrer, K., Weimer, S., Jimenez, J. L., Demerjian, K. L., Borrmann, S., and Worsnop, D. R.: A New Time-of-Flight Aerosol Mass Spectrometer (TOF-AMS)—Instrument Description and First Field Deployment, Aerosol Science and Technology, 39, 637–658, 10.1080/02786820500182040, 2005.
Drugé, T., Nabat, P., Mallet, M., Michou, M., Rémy, S., and Dubovik, O.: Modeling radiative and climatic effects of brown carbon aerosols with the ARPEGE-Climat global climate model, Atmos. Chem. Phys., 22, 12167–12205, 10.5194/acp-22-12167-2022, 2022.
Eom, S., Park, S. S., Liu, X., Oxford, C. R., Martin, R. V., Kim, J., and Song, C.-K.: Impact of Chemical Composition on Aerosol Scattering: Insights from the Surface Particulate Matter Network and Aerosol Robotic Network, Environmental Science & Technology, 59, 19899–19909, 10.1021/acs.est.5c09325, 2025.
Farmer, D. K., Cappa, C. D., and Kreidenweis, S. M.: Atmospheric Processes and Their Controlling Influence on Cloud Condensation Nuclei Activity, Chemical Reviews, 115, 4199–4217, 10.1021/cr5006292, 2015.
Farmer, D. K., Matsunaga, A., Docherty, K. S., Surratt, J. D., Seinfeld, J. H., Ziemann, P. J., and Jimenez, J. L.: Response of an aerosol mass spectrometer to organonitrates and organosulfates and implications for atmospheric chemistry, Proceedings of the National Academy of Sciences, 107, 6670–6675, 10.1073/pnas.0912340107, 2010.
Flores, J. M., Zhao, D. F., Segev, L., Schlag, P., Kiendler-Scharr, A., Fuchs, H., Watne, Å. K., Bluvshtein, N., Mentel, T. F., Hallquist, M., and Rudich, Y.: Evolution of the complex refractive index in the UV spectral region in ageing secondary organic aerosol, Atmos. Chem. Phys., 14, 5793–5806, 10.5194/acp-14-5793-2014, 2014.
Flowers, B. A., Dubey, M. K., Mazzoleni, C., Stone, E. A., Schauer, J. J., Kim, S. W., and Yoon, S. C.: Optical-chemical-microphysical relationships and closure studies for mixed carbonaceous aerosols observed at Jeju Island; 3-laser photoacoustic spectrometer, particle sizing, and filter analysis, Atmos. Chem. Phys., 10, 10387–10398, 10.5194/acp-10-10387-2010, 2010.
Formenti, P., Rajot, J. L., Desboeufs, K., Saïd, F., Grand, N., Chevaillier, S., and Schmechtig, C.: Airborne observations of mineral dust over western Africa in the summer Monsoon season: spatial and vertical variability of physico-chemical and optical properties, Atmos. Chem. Phys., 11, 6387–6410, 10.5194/acp-11-6387-2011, 2011.
Freney, E. J., Sellegri, K., Canonaco, F., Colomb, A., Borbon, A., Michoud, V., Doussin, J. F., Crumeyrolle, S., Amarouche, N., Pichon, J. M., Bourianne, T., Gomes, L., Prevot, A. S. H., Beekmann, M., and Schwarzenböeck, A.: Characterizing the impact of urban emissions on regional aerosol particles: airborne measurements during the MEGAPOLI experiment, Atmos. Chem. Phys., 14, 1397–1412, 10.5194/acp-14-1397-2014, 2014.

https://doi.org/10.5194/egusphere-2026-3147
Preprint. Discussion started: 25 June 2026

Fröhlich, R., Cubison, M. J., Slowik, J. G., Bukowiecki, N., Prévôt, A. S. H., Baltensperger, U., Schneider, J., Kimmel, J. R., Gonin, M., Rohner, U., Worsnop, D. R., and Jayne, J. T.: The ToF-ACSM: a portable aerosol chemical speciation monitor with TOFMS detection, Atmos. Meas. Tech., 6, 3225–3241, 10.5194/amt-6-3225-2013, 2013.

Goetz, J. D., Giordano, M. R., Stockwell, C. E., Bhave, P. V., Puppala, P. S., Panday, A. K., Jayarathne, T., Stone, E. A., Yokelson, R. J., and DeCarlo, P. F.: Aerosol Mass Spectral Profiles from NAMaSTE Field-Sampled South Asian Combustion Sources, ACS Earth and Space Chemistry, 6, 2619–2631, 10.1021/acsearthspacechem.2c00173, 2022.

Goetz, J. D., Giordano, M. R., Stockwell, C. E., Christian, T. J., Maharjan, R., Adhikari, S., Bhave, P. V., Praveen, P. S., Panday, A. K., Jayarathne, T., Stone, E. A., Yokelson, R. J., and DeCarlo, P. F.: Speciated online PM1 from South Asian combustion sources – Part 1: Fuel-based emission factors and size distributions, Atmos. Chem. Phys., 18, 14653–14679, 10.5194/acp-18-14653-2018, 2018.

Grange, S. K., Lee, J. D., Drysdale, W. S., Lewis, A. C., Hueglin, C., Emmenegger, L., and Carslaw, D. C.: COVID-19 lockdowns highlight a risk of increasing ozone pollution in European urban areas, Atmos. Chem. Phys., 21, 4169–4185, 10.5194/acp-21-4169-2021, 2021.

Grzegorski, M., Poli, G., Cacciari, A., Jafariserajehlou, S., Holdak, A., Lang, R., Vazquez-Navarro, M., Munro, R., and Fougnie, B.: Multi-Sensor Retrieval of Aerosol Optical Properties for Near-Real-Time Applications Using the Metop Series of Satellites: Concept, Detailed Description, and First Validation, 10.3390/rs14010085, 2022.

Harrison, R. M., Beddows, D. C. S., Alam, M. S., Singh, A., Brean, J., Xu, R., Kotthaus, S., and Grimmond, S.: Interpretation of particle number size distributions measured across an urban area during the FASTER campaign, Atmos. Chem. Phys., 19, 39–55, 10.5194/acp-19-39-2019, 2019.

Hayes, P. L., Ortega, A. M., Cubison, M. J., Froyd, K. D., Zhao, Y., Cliff, S. S., Hu, W. W., Toohey, D. W., Flynn, J. H., Lefer, B. L., Grossberg, N., Alvarez, S., Rappenglück, B., Taylor, J. W., Allan, J. D., Holloway, J. S., Gilman, J. B., Kuster, W. C., de Gouw, J. A., Massoli, P., Zhang, X., Liu, J., Weber, R. J., Corrigan, A. L., Russell, L. M., Isaacman, G., Worton, D. R., Kreisberg, N. M., Goldstein, A. H., Thalman, R., Waxman, E. M., Volkamer, R., Lin, Y. H., Surratt, J. D., Kleindienst, T. E., Offenberg, J. H., Dusanter, S., Griffith, S., Stevens, P. S., Brioude, J., Angevine, W. M., and Jimenez, J. L.: Organic aerosol composition and sources in Pasadena, California, during the 2010 CalNex campaign, Journal of Geophysical Research: Atmospheres, 118, 9233–9257, https://doi.org/10.1002/jgrd.50530, 2013.

He, Q., Tomaz, S., Li, C., Zhu, M., Meidan, D., Riva, M., Laskin, A., Brown, S. S., George, C., Wang, X., and Rudich, Y.: Optical Properties of Secondary Organic Aerosol Produced by Nitrate Radical Oxidation of Biogenic Volatile Organic Compounds, Environmental Science & Technology, 55, 2878–2889, 10.1021/acs.est.0c06838, 2021.

Herrera, M. E., Dubovik, O., Torres, B., Lapyonok, T., Fuertes, D., Lopatin, A., Litvinov, P., Chen, C., Benavent-Oltra, J. A., Bali, J. L., and Ristori, P. R.: Estimates of remote sensing retrieval errors by the GRASP algorithm: application to ground-based observations, concept and validation, Atmospheric Measurement Techniques, 15, 6075–6126, 10.5194/amt-15-6075-2022, 2022.

Jathar, S. H., Woody, M., Pye, H. O. T., Baker, K. R., and Robinson, A. L.: Chemical transport model simulations of organic aerosol in southern California: model evaluation and gasoline and diesel source contributions, Atmos. Chem. Phys., 17, 4305–4318, 10.5194/acp-17-4305-2017, 2017.

Jiang, X., Xue, Y., de Leeuw, G., Jin, C., Zhang, S., Sun, Y., and Wu, S.: Retrieval of hourly aerosol single scattering albedo over land using geostationary satellite data, npj Climate and Atmospheric Science, 7, 157, 10.1038/s41612-024-00690-6, 2024.

Jimenez, J. L., Canagaratna, M. R., Donahue, N. M., Prevot, A. S. H., Zhang, Q., Kroll, J. H., DeCarlo, P. F., Allan, J. D., Coe, H., Ng, N. L., Aiken, A. C., Docherty, K. S., Ulbrich, I. M., Grieshop, A. P., Robinson, A. L., Duplissy, J., Smith, J. D., Wilson, K. R., Lanz, V. A., Hueglin, C., Sun, Y. L., Tian, J., Laaksonen, A., Raatikainen, T., Rautiainen, J., Vaattovaara, P., Ehn, M., Kulmala, M., Tomlinson, J. M., Collins, D. R., Cubison, M. J., E, Dunlea, J., Huffman, J. A., Onasch, T. B., Alfarra, M. R., Williams, P. I., Bower, K., Kondo, Y., Schneider, J., Drewnick, F., Borrmann, S., Weimer, S., Demerjian, K., Salcedo, D., Cottrell, L., Griffin, R., Takami, A., Miyoshi, T., Hatakeyama, S., Shimono, A., Sun, J. Y., Zhang, Y. M., Dzepina, K., Kimmel, J. R., Sueper, D., Jayne, J. T., Herndon, S. C., Trimborn, A. M., Williams, L. R., Wood, E. C., Middlebrook, A. M., Kolb, C. E., Baltensperger, U., and Worsnop, D. R.: Evolution of Organic Aerosols in the Atmosphere, Science, 326, 1525–1529, 10.1126/science.1180353, 2009.

Jones, A., Thomson, D., Hort, M., and Devenish, B.: The U.K. Met Office's Next-Generation Atmospheric Dispersion Model, NAME III, Air Pollution Modeling and Its Application XVII, Boston, MA, 2007//, 580–589,

https://doi.org/10.5194/egusphere-2026-3147
Preprint. Discussion started: 25 June 2026

Kahn, R. A., Andrews, E., Brock, C. A., Chin, M., Feingold, G., Gettelman, A., Levy, R. C., Murphy, D. M., Nenes, A., Pierce, J. R., Popp, T., Redemann, J., Sayer, A. M., da Silva, A. M., Sogacheva, L., and Stier, P.: Reducing Aerosol Forcing Uncertainty by Combining Models With Satellite and Within-The-Atmosphere Observations: A Three-Way Street, Reviews of Geophysics, 61, e2022RG000796, https://doi.org/10.1029/2022RG000796, 2023.

Karagulian, F., Belis, C. A., Dora, C. F. C., Prüss-Ustün, A. M., Bonjour, S., Adair-Rohani, H., and Amann, M.: Contributions to cities' ambient particulate matter (PM): A systematic review of local source contributions at global level, Atmospheric Environment, 120, 475–483, https://doi.org/10.1016/j.atmosenv.2015.08.087, 2015.

Konovalov, I. B., Golovushkin, N. A., Beekmann, M., and Andreae, M. O.: Insights into the aging of biomass burning aerosol from satellite observations and 3D atmospheric modeling: evolution of the aerosol optical properties in Siberian wildfire plumes, Atmos. Chem. Phys., 21, 357–392, 10.5194/acp-21-357-2021, 2021.

Konwar, M., Werden, B., Fortner, E. C., Bera, S., Varghese, M., Chowdhuri, S., Hibert, K., Croteau, P., Jayne, J., Canagaratna, M., Malap, N., Jayakumar, S., Dixit, S. A., Murugavel, P., Axisa, D., Baumgardner, D., DeCarlo, P. F., Worsnop, D. R., and Prabhakaran, T.: Identifying the seeding signature in cloud particles from hydrometeor residuals, Atmos. Meas. Tech., 17, 2387–2400, 10.5194/amt-17-2387-2024, 2024.

Laing, J. R., Jaffe, D. A., and Sedlacek, I. I. I. A. J.: Comparison of Filter-based Absorption Measurements of Biomass Burning Aerosol and Background Aerosol at the Mt. Bachelor Observatory, Aerosol and Air Quality Research, 20, 663–678, 10.4209/aaqr.2019.06.0298, 2020.

Langridge, J. M., Lack, D., Brock, C. A., Bahreini, R., Middlebrook, A. M., Neuman, J. A., Nowak, J. B., Perring, A. E., Schwarz, J. P., Spackman, J. R., Holloway, J. S., Pollack, I. B., Ryerson, T. B., Roberts, J. M., Warneke, C., de Gouw, J. A., Trainer, M. K., and Murphy, D. M.: Evolution of aerosol properties impacting visibility and direct climate forcing in an ammonia-rich urban environment, Journal of Geophysical Research: Atmospheres, 117, https://doi.org/10.1029/2011JD017116, 2012.

Laskin, A., Laskin, J., and Nizkorodov, S. A.: Chemistry of Atmospheric Brown Carbon, Chemical Reviews, 115, 4335–4382, 10.1021/cr5006167, 2015.

Levy, R. C., Remer, L. A., and Dubovik, O.: Global aerosol optical properties and application to Moderate Resolution Imaging Spectroradiometer aerosol retrieval over land, Journal of Geophysical Research: Atmospheres, 112, https://doi.org/10.1029/2006JD007815, 2007.

Li, C., van Donkelaar, A., Hammer, M. S., McDuffie, E. E., Burnett, R. T., Spadaro, J. V., Chatterjee, D., Cohen, A. J., Apte, J. S., Southerland, V. A., Anenberg, S. C., Brauer, M., and Martin, R. V.: Reversal of trends in global fine particulate matter air pollution, Nature Communications, 14, 5349, 10.1038/s41467-023-41086-z, 2023.

Li, H., Zhang, Q., Zheng, B., Chen, C., Wu, N., Guo, H., Zhang, Y., Zheng, Y., Li, X., and He, K.: Nitrate-driven urban haze pollution during summertime over the North China Plain, Atmos. Chem. Phys., 18, 5293–5306, 10.5194/acp-18-5293-2018, 2018.

Li, J., Carlson, B. E., Yung, Y. L., Lv, D., Hansen, J., Penner, J. E., Liao, H., Ramaswamy, V., Kahn, R. A., Zhang, P., Dubovik, O., Ding, A., Lacis, A. A., Zhang, L., and Dong, Y.: Scattering and absorbing aerosols in the climate system, Nature Reviews Earth & Environment, 3, 363–379, 10.1038/s43017-022-00296-7, 2022a.

Li, L., Derimian, Y., Chen, C., Zhang, X., Che, H., Schuster, G. L., Fuertes, D., Litvinov, P., Lapyonok, T., Lopatin, A., Matar, C., Ducos, F., Karol, Y., Torres, B., Gui, K., Zheng, Y., Liang, Y., Lei, Y., Zhu, J., Zhang, L., Zhong, J., Zhang, X., and Dubovik, O.: Climatology of aerosol component concentrations derived from multi-angular polarimetric POLDER-3 observations using GRASP algorithm, Earth Syst. Sci. Data, 14, 3439–3469, 10.5194/essd-14-3439-2022, 2022b.

Manisalidis, I., Stavropoulou, E., Stavropoulos, A., and Bezirtzoglou, E.: Environmental and Health Impacts of Air Pollution: A Review, Front Public Health, 8, 14, 10.3389/fpubh.2020.00014, 2020.

McMeeking, G. R., Bart, M., Chazette, P., Haywood, J. M., Hopkins, J. R., McQuaid, J. B., Morgan, W. T., Raut, J. C., Ryder, C. L., Savage, N., Turnbull, K., and Coe, H.: Airborne measurements of trace gases and aerosols over the London metropolitan region, Atmos. Chem. Phys., 12, 5163–5187, 10.5194/acp-12-5163-2012, 2012.

Morgan, W. T., Allan, J. D., Bower, K. N., Highwood, E. J., Liu, D., McMeeking, G. R., Northway, M. J., Williams, P. I., Krejci, R., and Coe, H.: Airborne measurements of the spatial distribution of aerosol chemical composition across Europe and evolution of the organic fraction, Atmos. Chem. Phys., 10, 4065–4083, 10.5194/acp-10-4065-2010, 2010.

Nault, B. A., Campuzano-Jost, P., Day, D. A., Schroder, J. C., Anderson, B., Beyersdorf, A. J., Blake, D. R., Brune, W. H., Choi, Y., Corr, C. A., de Gouw, J. A., Dibb, J., DiGangi, J. P., Diskin, G. S., Fried, A., Huey, L. G., Kim, M. J., Knote, C. J.,

https://doi.org/10.5194/egusphere-2026-3147
Preprint. Discussion started: 25 June 2026

Lamb, K. D., Lee, T., Park, T., Pusede, S. E., Scheuer, E., Thornhill, K. L., Woo, J. H., and Jimenez, J. L.: Secondary organic aerosol production from local emissions dominates the organic aerosol budget over Seoul, South Korea, during KORUS-AQ, Atmos. Chem. Phys., 18, 17769–17800, 10.5194/acp-18-17769-2018, 2018.

Nault, B. A., Jo, D. S., McDonald, B. C., Campuzano-Jost, P., Day, D. A., Hu, W., Schroder, J. C., Allan, J., Blake, D. R., Canagaratna, M. R., Coe, H., Coggon, M. M., DeCarlo, P. F., Diskin, G. S., Dunmore, R., Flocke, F., Fried, A., Gilman, J. B., Gkatzelis, G., Hamilton, J. F., Hanisco, T. F., Hayes, P. L., Henze, D. K., Hodzic, A., Hopkins, J., Hu, M., Huey, L. G., Jobson, B. T., Kuster, W. C., Lewis, A., Li, M., Liao, J., Nawaz, M. O., Pollack, I. B., Peischl, J., Rappenglück, B., Reeves, C. E., Richter, D., Roberts, J. M., Ryerson, T. B., Shao, M., Sommers, J. M., Walega, J., Warneke, C., Weibring, P., Wolfe, G. M., Young, D. E., Yuan, B., Zhang, Q., de Gouw, J. A., and Jimenez, J. L.: Secondary organic aerosols from anthropogenic volatile organic compounds contribute substantially to air pollution mortality, Atmos. Chem. Phys., 21, 11201–11224, 10.5194/acp-21-11201-2021, 2021.

Onasch, T. B., Massoli, P., Kebabian, P. L., Hills, F. B., Bacon, F. W., and Freedman, A.: Single Scattering Albedo Monitor for Airborne Particulates, Aerosol Science and Technology, 49, 267–279, 10.1080/02786826.2015.1022248, 2015.

Pereira, D. L., Giorio, C., Gratien, A., Zherebker, A., Noyalet, G., Chevaillier, S., Alage, S., Almarj, E., Bergé, A., Bertin, T., Cazaunau, M., Coll, P., Di Antonio, L., Harb, S., Heuser, J., Gaimoz, C., Guillemant, O., Language, B., Lauret, O., Macias, C., Maisonneuve, F., Picquet-Varrault, B., Torres, R., Triquet, S., Zapf, P., Hawkins, L., Pronovost, D., Riley, S., Flaud, P. M., Perraudin, E., Pouyes, P., Villenave, E., Albinet, A., Favez, O., Aujay-Plouzeau, R., Michoud, V., Cantrell, C., Cirtog, M., Di Biagio, C., Doussin, J. F., and Formenti, P.: Molecular characterization of organic aerosols in urban and forested areas of Paris using high-resolution mass spectrometry, Atmos. Chem. Phys., 25, 4885–4905, 10.5194/acp-25-4885-2025, 2025.

Petzold, A., Ogren, J. A., Fiebig, M., Laj, P., Li, S. M., Baltensperger, U., Holzer-Popp, T., Kinne, S., Pappalardo, G., Sugimoto, N., Wehrli, C., Wiedensohler, A., and Zhang, X. Y.: Recommendations for reporting "black carbon" measurements, Atmos. Chem. Phys., 13, 8365–8379, 10.5194/acp-13-8365-2013, 2013.

Pieber, S. M., El Haddad, I., Slowik, J. G., Canagaratna, M. R., Jayne, J. T., Platt, S. M., Bozzetti, C., Daellenbach, K. R., Fröhlich, R., Vlachou, A., Klein, F., Dommen, J., Miljevic, B., Jiménez, J. L., Worsnop, D. R., Baltensperger, U., and Prévôt, A. S. H.: Inorganic Salt Interference on CO2+ in Aerodyne AMS and ACSM Organic Aerosol Composition Studies, Environmental Science & Technology, 50, 10494–10503, 10.1021/acs.est.6b01035, 2016.

Raut, J. C. and Chazette, P.: Vertical profiles of urban aerosol complex refractive index in the frame of ESQUIF airborne measurements, Atmos. Chem. Phys., 8, 901–919, 10.5194/acp-8-901-2008, 2008.

Ravishankara, A. R., Rudich, Y., and Wuebbles, D. J.: Physical Chemistry of Climate Metrics, Chemical Reviews, 115, 3682–3703, 10.1021/acs.chemrev.5b00010, 2015.

Riemer, N., Ault, A. P., West, M., Craig, R. L., and Curtis, J. H.: Aerosol Mixing State: Measurements, Modeling, and Impacts, Reviews of Geophysics, 57, 187–249, https://doi.org/10.1029/2018RG000615, 2019.

Savadkoohi, M., Pandolfi, M., Reche, C., Niemi, J. V., Mooibroek, D., Titos, G., Green, D. C., Tremper, A. H., Hueglin, C., Liakakou, E., Mihalopoulos, N., Stavroulas, I., Artiñano, B., Coz, E., Alados-Arboledas, L., Beddows, D., Riffault, V., De Brito, J. F., Bastian, S., Baudic, A., Colombi, C., Costabile, F., Chazeau, B., Marchand, N., Gómez-Amo, J. L., Estellés, V., Matos, V., van der Gaag, E., Gille, G., Luoma, K., Manninen, H. E., Norman, M., Silvergren, S., Petit, J.-E., Putaud, J.-P., Rattigan, O. V., Timonen, H., Tuch, T., Merkel, M., Weinhold, K., Vratolis, S., Vasilescu, J., Favez, O., Harrison, R. M., Laj, P., Wiedensohler, A., Hopke, P. K., Petäjä, T., Alastuey, A., and Querol, X.: The variability of mass concentrations and source apportionment analysis of equivalent black carbon across urban Europe, Environment International, 178, 108081, https://doi.org/10.1016/j.envint.2023.108081, 2023.

Schroder, J. C., Campuzano-Jost, P., Day, D. A., Shah, V., Larson, K., Sommers, J. M., Sullivan, A. P., Campos, T., Reeves, J. M., Hills, A., Hornbrook, R. S., Blake, N. J., Scheuer, E., Guo, H., Fibiger, D. L., McDuffie, E. E., Hayes, P. L., Weber, R. J., Dibb, J. E., Apel, E. C., Jaeglé, L., Brown, S. S., Thornton, J. A., and Jimenez, J. L.: Sources and Secondary Production of Organic Aerosols in the Northeastern United States during WINTER, Journal of Geophysical Research: Atmospheres, 123, 7771–7796, https://doi.org/10.1029/2018JD028475, 2018.

Shen, J., Kuang, Y., Liu, L., Yuan, F., Luo, B., Qiao, H., Zhai, M., Zhao, G., Xu, H., Li, F., Zou, Y., Deng, T., and Deng, X.: Refractive index enhancement by secondary organic aerosol formation in humid southern China challenges model assumptions, Atmos. Chem. Phys., 25, 11233–11246, 10.5194/acp-25-11233-2025, 2025.

https://doi.org/10.5194/egusphere-2026-3147
Preprint. Discussion started: 25 June 2026

Shepherd, R. H., King, M. D., Marks, A. A., Brough, N., and Ward, A. D.: Determination of the refractive index of insoluble organic extracts from atmospheric aerosol over the visible wavelength range using optical tweezers, Atmos. Chem. Phys., 18, 5235–5252, 10.5194/acp-18-5235-2018, 2018.

Shilling, J. E., Pekour, M. S., Fortner, E. C., Artaxo, P., de Sá, S., Hubbe, J. M., Longo, K. M., Machado, L. A. T., Martin, S. T., Springston, S. R., Tomlinson, J., and Wang, J.: Aircraft observations of the chemical composition and aging of aerosol in the Manaus urban plume during GoAmazon 2014/5, Atmos. Chem. Phys., 18, 10773–10797, 10.5194/acp-18-10773-2018, 2018.

Shingler, T., Crosbie, E., Ortega, A., Shiraiwa, M., Zuend, A., Beyersdorf, A., Ziemba, L., Anderson, B., Thornhill, L., Perring, A. E., Schwarz, J. P., Campazano-Jost, P., Day, D. A., Jimenez, J. L., Hair, J. W., Mikoviny, T., Wisthaler, A., and Sorooshian, A.: Airborne characterization of subsaturated aerosol hygroscopicity and dry refractive index from the surface to 6.5 km during the SEAC4RS campaign, Journal of Geophysical Research: Atmospheres, 121, 4188–4210, https://doi.org/10.1002/2015JD024498, 2016.

Taylor, J. W., Allan, J. D., Liu, D., Flynn, M., Weber, R., Zhang, X., Lefer, B. L., Grossberg, N., Flynn, J., and Coe, H.: Assessment of the sensitivity of core / shell parameters derived using the single-particle soot photometer to density and refractive index, Atmos. Meas. Tech., 8, 1701–1718, 10.5194/amt-8-1701-2015, 2015.

Teri, M., Müller, T., Gasteiger, J., Valentini, S., Horvath, H., Vecchi, R., Bauer, P., Walser, A., and Weinzierl, B.: Impact of particle size, refractive index, and shape on the determination of the particle scattering coefficient – an optical closure study evaluating different nephelometer angular truncation and illumination corrections, Atmospheric Measurement Techniques, 15, 3161–3187, 10.5194/amt-15-3161-2022, 2022.

Tian, P., Liu, D., Zhao, D., Yu, C., Liu, Q., Huang, M., Deng, Z., Ran, L., Wu, Y., Ding, S., Hu, K., Zhao, G., Zhao, C., and Ding, D.: In situ vertical characteristics of optical properties and heating rates of aerosol over Beijing, Atmos. Chem. Phys., 20, 2603–2622, 10.5194/acp-20-2603-2020, 2020.

Tinorua, S., Denjean, C., Nabat, P., Bourrianne, T., Pont, V., Gheusi, F., and Leclerc, E.: Higher absorption enhancement of black carbon in summer shown by 2-year measurements at the high-altitude mountain site of Pic du Midi Observatory in the French Pyrenees, Atmos. Chem. Phys., 24, 1801–1824, 10.5194/acp-24-1801-2024, 2024a.

Tinorua, S., Denjean, C., Nabat, P., Pont, V., Arnaud, M., Bourrianne, T., Dias Alves, M., and Gardrat, E.: A 2-year intercomparison of three methods for measuring black carbon concentration at a high-altitude research station in Europe, Atmos. Meas. Tech., 17, 3897–3915, 10.5194/amt-17-3897-2024, 2024b.

Tsigaridis, K. and Kanakidou, M.: The Present and Future of Secondary Organic Aerosol Direct Forcing on Climate, Current Climate Change Reports, 4, 84–98, 10.1007/s40641-018-0092-3, 2018.

Tsigaridis, K., Daskalakis, N., Kanakidou, M., Adams, P. J., Artaxo, P., Bahadur, R., Balkanski, Y., Bauer, S. E., Bellouin, N., Benedetti, A., Bergman, T., Berntsen, T. K., Beukes, J. P., Bian, H., Carslaw, K. S., Chin, M., Curci, G., Diehl, T., Easter, R. C., Ghan, S. J., Gong, S. L., Hodzic, A., Hoyle, C. R., Iversen, T., Jathar, S., Jimenez, J. L., Kaiser, J. W., Kirkevåg, A., Koch, D., Kokkola, H., Lee, Y. H., Lin, G., Liu, X., Luo, G., Ma, X., Mann, G. W., Mihalopoulos, N., Morcrette, J. J., Müller, J. F., Myhre, G., Myriokefalitakis, S., Ng, N. L., O'Donnell, D., Penner, J. E., Pozzoli, L., Pringle, K. J., Russell, L. M., Schulz, M., Sciare, J., Seland, Ø., Shindell, D. T., Sillman, S., Skeie, R. B., Spracklen, D., Stavrakou, T., Steenrod, S. D., Takemura, T., Tiitta, P., Tilmes, S., Tost, H., van Noije, T., van Zyl, P. G., von Salzen, K., Yu, F., Wang, Z., Wang, Z., Zaveri, R. A., Zhang, H., Zhang, K., Zhang, Q., and Zhang, X.: The AeroCom evaluation and intercomparison of organic aerosol in global models, Atmos. Chem. Phys., 14, 10845–10895, 10.5194/acp-14-10845-2014, 2014.

Tsimpidi, A. P., Scholz, S. M. C., Milousis, A., Mihalopoulos, N., and Karydis, V. A.: Aerosol composition trends during 2000–2020: in-depth insights from model predictions and multiple worldwide near-surface observation datasets, Atmos. Chem. Phys., 25, 10183–10213, 10.5194/acp-25-10183-2025, 2025.

Velazquez-Garcia, A., Denjean, C., Yu, C., Tinorua, S., Bourrianne, T., Burnet, F., Tu, K., Pangui, E., Pereira, D. L., Cazaunau, M., Di Antonio, L., Siour, G., Beekmann, M., DeCarlo, P. F., Nault, B. A., Bauville, A., Cantrell, C., Formenti, P., and Michoud, V.: Observational Evidence for Relative Humidity Driving Black Carbon Mixing State and Absorption Enhancement in Urban Outflows, Geophysical Research Letters, 53, e2025GL121520, https://doi.org/10.1029/2025GL121520, 2026.

von der Weiden, S. L., Drewnick, F., and Borrmann, S.: Particle Loss Calculator – a new software tool for the assessment of the performance of aerosol inlet systems, Atmos. Meas. Tech., 2, 479–494, 10.5194/amt-2-479-2009, 2009.

Vu, K. T., Dingle, J. H., Bahreini, R., Reddy, P. J., Apel, E. C., Campos, T. L., DiGangi, J. P., Diskin, G. S., Fried, A., Herndon, S. C., Hills, A. J., Hornbrook, R. S., Huey, G., Kaser, L., Montzka, D. D., Nowak, J. B., Pusede, S. E., Richter, D., Roscioli,

https://doi.org/10.5194/egusphere-2026-3147
Preprint. Discussion started: 25 June 2026

J. R., Sachse, G. W., Shertz, S., Stell, M., Tanner, D., Tyndall, G. S., Walega, J., Weibring, P., Weinheimer, A. J., Pfister, G., and Flocke, F.: Impacts of the Denver Cyclone on regional air quality and aerosol formation in the Colorado Front Range during FRAPPÉ 2014, Atmos. Chem. Phys., 16, 12039–12058, 10.5194/acp-16-12039-2016, 2016.

Weber, P., Petzold, A., Bischof, O. F., Fischer, B., Berg, M., Freedman, A., Onasch, T. B., and Bundke, U.: Relative errors in derived multi-wavelength intensive aerosol optical properties using cavity attenuated phase shift single-scattering albedo monitors, a nephelometer, and tricolour absorption photometer measurements, Atmos. Meas. Tech., 15, 3279–3296, 10.5194/amt-15-3279-2022, 2022.

Werden, B. S., Giordano, M. R., Mahata, K., Islam, M. R., Goetz, J. D., Puppala, S. P., Saikawa, E., Panday, A. K., Yokelson, R. J., Stone, E. A., and DeCarlo, P. F.: Submicron Aerosol Composition and Source Contribution across the Kathmandu Valley, Nepal, in Winter, ACS Earth and Space Chemistry, 7, 49–68, 10.1021/acsearthspacechem.2c00226, 2023.

Wu, Y., Li, J., Xia, Y., Deng, Z., Tao, J., Tian, P., Gao, Z., Xia, X., and Zhang, R.: Size-resolved refractive index of scattering aerosols in urban Beijing: A seasonal comparison, Aerosol Science and Technology, 55, 1070–1083, 10.1080/02786826.2021.1924357, 2021.

Wu, Y., Liu, D., Tian, P., Sheng, J., Liu, Q., Li, R., Hu, K., Jiang, X., Li, S., Bi, K., Zhao, D., Huang, M., Ding, D., and Wang, J.: Tracing the Formation of Secondary Aerosols Influenced by Solar Radiation and Relative Humidity in Suburban Environment, Journal of Geophysical Research: Atmospheres, 127, e2022JD036913, https://doi.org/10.1029/2022JD036913, 2022.

Yu, C., Pangui, E., Tu, K., Cazaunau, M., Feingesicht, M., Xavier, L., Bourrianne, T., Michoud, V., Cantrell, C., Onasch, T. B., Freedman, A., and Formenti, P.: Characterisation of particle single-scattering albedo with a modified airborne dual-wavelength CAPS monitor, Atmospheric Measurement Techniques, 17, 3419–3437, 10.5194/amt-17-3419-2024, 2024.

Yu, C., Pasternak, D., Lee, J., Yang, M., Bell, T., Bower, K., Wu, H., Liu, D., Reed, C., Bauguitte, S., Cliff, S., Trembath, J., Coe, H., and Allan, J. D.: Characterizing the Particle Composition and Cloud Condensation Nuclei from Shipping Emission in Western Europe, Environmental Science & Technology, 54, 15604–15612, 10.1021/acs.est.0c04039, 2020.

Yu, C., Formenti, P., de Brito, J. F., Bauville, A., Bergé, A., Bouzidi, H., Cazaunau, M., Cirtog, M., Di Biagio, C., Di Antonio, L., Gaimoz, C., Maisonneuve, F., Zapf, P., Seubert, T., Andersen, S. T., Dewald, P., Türk, G. N. T. E., Crowley, J. N., Kukui, A., Xue, C., Denjean, C., Garrouste, O., Etienne, J. C., Wu, H., Allan, J. D., Liu, D., Wu, Y., Cantrell, C., and Michoud, V.: Impacts of summertime photochemical aging on the physicochemical properties of aerosols in a Paris suburban forest region, EGUsphere, 2025, 1–28, 10.5194/egusphere-2025-2667, 2025.

Yus-Díez, J., Bernardoni, V., Močnik, G., Alastuey, A., Ciniglia, D., Ivančič, M., Querol, X., Perez, N., Reche, C., Rigler, M., Vecchi, R., Valentini, S., and Pandolfi, M.: Determination of the multiple-scattering correction factor and its cross-sensitivity to scattering and wavelength dependence for different AE33 Aethalometer filter tapes: a multi-instrumental approach, Atmos. Meas. Tech., 14, 6335–6355, 10.5194/amt-14-6335-2021, 2021.

Zaveri, R. A., Barnard, J. C., Easter, R. C., Riemer, N., and West, M.: Particle-resolved simulation of aerosol size, composition, mixing state, and the associated optical and cloud condensation nuclei activation properties in an evolving urban plume, Journal of Geophysical Research: Atmospheres, 115, https://doi.org/10.1029/2009JD013616, 2010.

Zaveri, R. A., Wang, J., Fan, J., Zhang, Y., Shilling, J. E., Zelenyuk, A., Mei, F., Newsom, R., Pekour, M., Tomlinson, J., Comstock, J. M., Shrivastava, M., Fortner, E., Machado, L. A. T., Artaxo, P., and Martin, S. T.: Rapid growth of anthropogenic organic nanoparticles greatly alters cloud life cycle in the Amazon rainforest, Science Advances, 8, eabj0329, 10.1126/sciadv.abj0329, 2022.

Zhang, H., Kondragunta, S., and Ciren, P.: TEMPO Aerosol Optical Depth and Aerosol Layer Height Retrieval Algorithm, Journal of Geophysical Research: Atmospheres, 130, e2025JD044082, https://doi.org/10.1029/2025JD044082, 2025.

Zhang, Q., Jimenez, J. L., Canagaratna, M. R., Allan, J. D., Coe, H., Ulbrich, I., Alfarra, M. R., Takami, A., Middlebrook, A. M., Sun, Y. L., Dzepina, K., Dunlea, E., Docherty, K., DeCarlo, P. F., Salcedo, D., Onasch, T., Jayne, J. T., Miyoshi, T., Shimono, A., Hatakeyama, S., Takegawa, N., Kondo, Y., Schneider, J., Drewnick, F., Borrmann, S., Weimer, S., Demerjian, K., Williams, P., Bower, K., Bahreini, R., Cottrell, L., Griffin, R. J., Rautiainen, J., Sun, J. Y., Zhang, Y. M., and Worsnop, D. R.: Ubiquity and dominance of oxygenated species in organic aerosols in anthropogenically-influenced Northern Hemisphere midlatitudes, Geophysical Research Letters, 34, https://doi.org/10.1029/2007GL029979, 2007.

Zhang, Q. J., Beekmann, M., Freney, E., Sellegri, K., Pichon, J. M., Schwarzenboeck, A., Colomb, A., Bourrianne, T., Michoud, V., and Borbon, A.: Formation of secondary organic aerosol in the Paris pollution plume and its impact on surrounding regions, Atmos. Chem. Phys., 15, 13973–13992, 10.5194/acp-15-13973-2015, 2015.